J. Fluid Mech. (1989), *vol.* 202, *pp.* 117–148
Printed in Great Britain

Numerical simulations of freely evolving turbulence in stably stratified fluids

By OLIVIER MÉTAIS†‡ AND JACKSON R. HERRING†

†National Center for Atmospheric Research, PO Box 3000, Boulder, CO 80307, USA

‡Institut de Mécanique de Grenoble, Domaine Universitaire, BP 53X, 38041 Grenoble Cedex, France

(Received 5 January 1988 and in revised form 3 October 1988)

Results of direct numerical simulations of stably stratified, freely evolving, homogeneous turbulence are presented. An examination of initial data designed to give insight into laboratory flows suggests that the numerical simulations have a satisfactory degree of realism, insofar as statistical parameters such as total energy and length scales are concerned. The motion is decomposed into a stratified turbulence (vortical) component and a wave component. For initial-value problems similar to laboratory studies of stratified flows, the vortical component decays at a rate virtually identical to that of the non-buoyant case up to $t = 6N^{-1}$ (N is the Brunt–Väisälä frequency). The decay rate decreases after this time, suggesting a kind of turbulence 'collapse'. The temperature structure that emerges clearly shows the development of the collapse stage of the flow, which is also diagnosed by the behaviour of parameters such as the Thorpe scale.

We next examine the very small-Froude-number regime in order to understand possible universal aspects of the flow. An examination of various initial conditions with different proportions of stratified and wave components indicates a lack of universality. For initial data containing only vortical motion (motions derived from the vertical vorticity field), the vortical field tends to dominate, in subsequent evolution, at strong stratification. However, contrary to two-dimensional turbulence, the flow is more strongly dissipative than two-dimensional flows due to the frictional effect associated with layering. Other quantities examined are frequency spectra, and the probability distribution for vertical shear. The frequency spectra exhibit some features in common with spectra extracted from oceanographic data.

1. Introduction

Many laboratory experiments (see Hopfinger 1987 for a review) have examined the decay of three-dimensional turbulence in stably stratified fluids. These studies have shown that if the inertial forces are very small in comparison with buoyancy (small-Froude-number regime), the flow evolve towards a collapsed state in which internal gravity waves and stratified (quasi-two-dimensional) turbulence coexist. A theoretical analysis developed by Riley, Metcalfe & Weissman (1981) (hereafter referred to as RMW) and by Lilly (1983) suggested that stratified turbulence (also called the vortex or the potential vorticity component of the flow) could correspond to two-dimensional turbulence in almost independently evolving layers. However, the vertical variability of the vortical component induces gravity waves and these, in turn, inject energy into the vortical mode through nonlinear interactions. The schematics of these interactions have been described by Riley (1985). Further

theoretical work by Herring & Métais (1989) suggests that the stratified component, through its vertical variability, does indeed activate the wave component; but the former becomes progressively more dominant as (stable) stratification increases. Moreover, there exists the possibility of non-wave generalizations of two-dimensional turbulence in the limit of very small Froude number by means of the balanced equations as proposed by McWilliams (1985). Thus, the major issues to understand are the interactions between stratified turbulence and gravity waves, the dynamics of stratified turbulence (the degree to which ideas of two-dimensional cascade carry over the stratified component), and the role of vertical variability in providing a damping for the two-dimensional, vortical component.

Direct numerical simulations of the decay of initially isotropic homogeneous turbulence in a Boussinesq fluid have been performed by RMW. Although they observed a wave-like behaviour in the flow, they stressed that no sharp transition occurs as the flow evolves from a fully turbulent and dissipative state to a stratified state. However, the Reynolds number was too low to allow for a long period of decay or comparisons with experiments (such as Itsweire, Helland & Van Atta 1986). The present paper focuses on direct numerical simulations of the decay of homogeneous stratified turbulence, but for Reynolds number comparable with experiments. We note that, with respect to the major statistical descriptors of the flow, the direct numerical simulations and laboratory experiments are in fairly good agreement (§3.1). Therefore, we argue that the physics of numerical turbulence has sufficient realism to use direct numerical simulations to bring into direct scrutiny the nature of the flow's collapsed phase (§3.2). Section 3.3 is devoted to the decay of strongly stratified turbulence (small-Froude-number regime). Our results show that the statistical symmetry of the evolved state depends vitally on that of the initial data. Thus, for small Froude number, the flow evolves as stratified two-dimensional flow only if the initial wave component is small. Conversely, if the flow is initially wave dominated, it remains so throughout its decay. Further details concerning flow initially near equipartition are discussed in §3.3.

2. Methodology

2.1. *Equations of motion and relevant dynamical degrees of freedom*

The velocity and density fields examined here satisfy the Boussinesq set:

$$\left(\frac{\partial}{\partial t}-\nu\nabla^2\right)\boldsymbol{u} = -\boldsymbol{\nabla} p-(\boldsymbol{u}\cdot\boldsymbol{\nabla})\,\boldsymbol{u}-z\Theta, \tag{1}$$

$$\left(\frac{\partial}{\partial t}-\kappa\nabla^2\right)\Theta = N^2 w-(\boldsymbol{u}\cdot\boldsymbol{\nabla})\,\Theta, \tag{2}$$

$$\boldsymbol{\nabla}\cdot\boldsymbol{u} = 0. \tag{3}$$

ν and κ are, respectively, the kinematic molecular viscosity and diffusivity. x, y, z is a right-handed Cartesian coordinate system with z directed in the vertical. Θ is proportional to the density deviation ρ' from the mean density profile $\bar{\rho}(z)$; $\Theta = g\rho'/\rho_0$, with ρ_0 the volume-averaged value of $\bar{\rho}(z)$ and g the acceleration due to gravity (gravity vector: $\boldsymbol{g} = (0, 0, -g)$). $\boldsymbol{u} = (u, v, w)$ and ρ' are homogeneous. The (constant) Brunt–Väisälä frequency is

$$N = \left(-\frac{g}{\rho_0}\frac{\mathrm{d}\bar{\rho}}{\mathrm{d}z}\right)^{\frac{1}{2}}. \tag{4}$$

Craya (1958) introduced a decomposition of $\hat{\boldsymbol{u}}(\boldsymbol{k})$ (written in Fourier space) into the orthogonal components $\hat{\boldsymbol{u}}_1$ and $\hat{\boldsymbol{u}}_2$:

$$\hat{\boldsymbol{u}}(\boldsymbol{k},t) = \hat{\boldsymbol{u}}_1(\boldsymbol{k},t) + \hat{\boldsymbol{u}}_2(\boldsymbol{k},t), \tag{5}$$

with

$$\boldsymbol{u}_1(\boldsymbol{k},t) = \hat{\phi}_1(\boldsymbol{k},t)\,\boldsymbol{e}_1(\boldsymbol{k}), \tag{6}$$

$$\boldsymbol{u}_2(\boldsymbol{k},t) = \hat{\phi}_2(\boldsymbol{k},t)\,\boldsymbol{e}_2(\boldsymbol{k}), \tag{7}$$

where

$$\boldsymbol{e}_1(\boldsymbol{k}) = (\boldsymbol{k}\times\boldsymbol{g})/|(\boldsymbol{k}\times\boldsymbol{g})| \tag{8}$$

and

$$\boldsymbol{e}_2(\boldsymbol{k}) = \boldsymbol{k}\times(\boldsymbol{k}\times\boldsymbol{g})/|\boldsymbol{k}\times(\boldsymbol{k}\times\boldsymbol{g})|. \tag{9}$$

Here $\boldsymbol{k}$ is the wavenumber vector. RMW noticed that for small amplitudes (linear theory), $\hat{\boldsymbol{u}}_2$ (which has no vertical vorticity) satisfies the (linearized) propagation equation of internal gravity waves. By means of a suitable scale analysis of the equations of motion, (1)–(3) they indicated that $\hat{\boldsymbol{u}}_1$, which is the horizontally non-divergent rotational part of the velocity field, could, in the limit of infinitely small Froude numbers, satisfy the two-dimensional Navier–Stokes equations but with an undetermined z-dependence. The situation here (at low Froude number) is analogous to the case of turbulence coexisting with acoustics (at low Mach number), with two-dimensional turbulence playing the role of turbulence in the turbulence–acoustic analogue.

For invariantly identifying waves and turbulence, Ertel's theorem provides a useful basis. This theorem states that (for non-dissipative and non-diffusive flows) the potential vorticity ($\Pi \equiv (\boldsymbol{\omega}\cdot\nabla\rho)/\rho_0$) is conserved along fluid-parcel trajectories. Here, $\boldsymbol{\omega}$ is the absolute vorticity which includes possible solid-body rotation, and $\rho = \bar{\rho}+\rho'$. Take the 'vortical' velocity such that its vorticity is normal to the constant-ρ surface, and the 'wave' as that component of $\boldsymbol{u}(\boldsymbol{x},t)$ normal to the vortical component and with vorticity in the isopycnal surface (which together with the vortical component comprises an incompressible field). A formulation of the stratified turbulence problem along these lines has been introduced by Staquet & Riley (1989). In such a description, the vortical component does not explicitly interact with the wave components. It does implicitly, though, since the billows in an isopycnal surface are determined by the amplitude of the waves. Such a description is, of course, formulated in an intrinsic Lagrangian frame, whereas that of ϕ_1, ϕ_2 introduced above is Eulerian: ϕ_1, ϕ_2 are, in fact, eigenmodes of the linear part of the problem. It can be an accurate means of identifying waves and turbulence only as $N\to\infty$, in which case the two descriptions become identical.

On the other hand, an appeal to Ertel's theorem alone as the basis for discussing waves versus turbulence seems deficient in incorporating the wave-propagation aspects of flow, since it would seem that a proper definition of waves should include the density field, and its phase relative to the 'wave'-component of the velocity. Furthermore, for unstratified flow, eventually ϕ_1 and ϕ_2 equipartition and the isopycnal surfaces become in time severely convoluted. One would not in this case claim that the vorticity in the isopycnal surface corresponds to waves.

From these considerations we conclude that ϕ_1, ϕ_2 should be regarded as an economical (and complete) Eulerian description of the flow, but not as an intrinsic method of identifying wave and vortical components. Only the limit $N\to\infty$, does it correspond to the Ertel's description, and thus invariably identify 'wave' and 'vortical' components of the flow.

Finally, we note that $(\hat{\boldsymbol{u}}_1, \hat{\boldsymbol{u}}_2)$ also represents a convenient representation of the turbulence, since for isotropic three-dimensional turbulence, we have $\boldsymbol{\Phi}_1(\boldsymbol{k}) = \boldsymbol{\Phi}_2(\boldsymbol{k})$,

and both are independent of the direction of $\boldsymbol{k}$. Also, stratification preserves axisymmetry, and the above decomposition serves as an economical description of the second-order velocity correlation tensor of axisymmetric turbulence (Herring 1974; Lesieur 1987). This property is also useful in applying statistical theories of turbulence (two-point closures) to the Boussinesq equations (Métais *et al.* 1987).

For convenience, we call $\Phi_1(\boldsymbol{k})$ the intensity associated with $\hat{\phi}_1$ the 'vortex' kinetic energy spectrum:

$$\Phi_1(\boldsymbol{k}) = \langle \hat{\phi}_1^*(\boldsymbol{k})\, \hat{\phi}_1(\boldsymbol{k}) \rangle \tag{10}$$

and $\Phi_2(\boldsymbol{k})$ the 'wave' kinetic energy spectrum. Here the brackets denote an ensemble average. We define the potential energy spectrum as

$$P(\boldsymbol{k}) = \frac{1}{2} \frac{\langle \Theta(-\boldsymbol{k})\, \Theta(\boldsymbol{k}) \rangle}{N^2}, \tag{11}$$

so that the total energy $\bar{\Phi}_1(t) + \bar{\Phi}_2(t) + \bar{P}(t)$ (where $\bar{\Phi}_1(t) = \int \Phi_1 \, \mathrm{d}\boldsymbol{k}$, etc.) is conserved by nonlinear terms in the equations of motion.

2.2. *Lengthscales*; *Reynolds, Froude and Richardson number*

We define the horizontal integral scale as

$$L_\mathrm{h} = \int_{-\infty}^{\infty} \mathrm{d}\zeta \langle \phi_1(x, y+\zeta, z)\, \phi_1(x, y, z) \rangle / \langle \phi_1^2 \rangle, \tag{12}$$

and the vertical integral scale as

$$L_\mathrm{v} = \int_{-\infty}^{\infty} \mathrm{d}\zeta \langle \phi_1(x, y, z+\zeta)\, \phi_1(x, y, z) \rangle / \langle \phi_1^2 \rangle. \tag{13}$$

These definitions (particularly (13)) are of course not unique (one could use in (13) ϕ_2, or any linear combination of ϕ_1 and ϕ_2), but they are conventional (RMW) and seem appropriate for flow in which the horizontal motion field (and hence ϕ_1) dominates. Assuming that in the small scales the flow is isotropic with a dissipation rate of kinetic energy ϵ, Dougherty (1961) and Ozmidov (1965) derived a characteristic lengthscale of stratification by equating inertial time $(L_\mathrm{R}^2/\epsilon)^{\frac{1}{3}}$ and the buoyant time N^{-1}:

$$L_\mathrm{R} = (\epsilon/N^3)^{\frac{1}{2}}. \tag{14}$$

An equivalent lengthscale (buoyancy lengthscale) can be defined by equating the vertical inertial time $((L_\mathrm{b}/\langle w^2 \rangle^{\frac{1}{2}}))$ to N^{-1}:

$$L_\mathrm{b} = \langle w^2 \rangle^{\frac{1}{2}} / N. \tag{15}$$

The largest vertical turbulent scale has been defined by Stillinger, Helland & Van Atta (1983) as

$$L_\mathrm{t} = 2\langle \Theta^2 \rangle^{\frac{1}{2}} / N^2, \tag{16}$$

and the classical Kolmogorov scale (balancing dissipative and inertial effects) is given by

$$L_\mathrm{K} = (\epsilon/\nu^3)^{\frac{1}{4}}. \tag{17}$$

A lengthscale characteristic of vertical overturning in a stratified flow has been derived by Thorpe (1977). It is commonly used in discussions of oceanographic microstructure data (Dillon 1982) and laboratory measurements (Itsweire 1984), and is called the displacement scale or Thorpe's scale. To better understand its definition, consider an instantaneous sounding $\rho_i(z)$. This may present convectively unstable

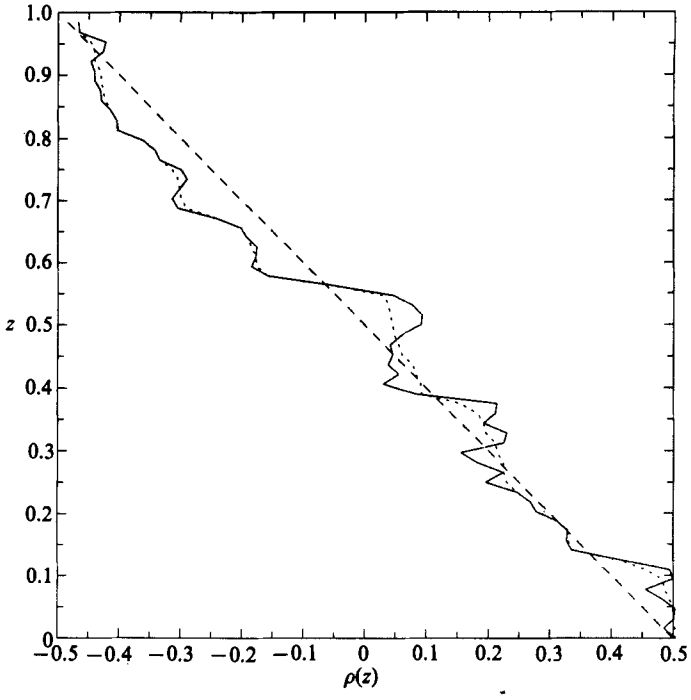

FIGURE 1. The initial vertical profile $\rho_i(z)$ (——) is rearranged using Thorpe's technique so that each fluid particle of the new profile $\rho_n(z)$ (· · · · ·) is stable.

regions (see figure 1). Next rearrange the profile so that each fluid particle of the new profile $\rho_n(z)$ is stable and

$$\int_{z_b}^{z_t} \rho_i(z)\,dz = \int_{z_b}^{z_t} \rho_n(z)\,dz, \tag{18}$$

where $z_t - z_b$ is the layer height. The Thorpe scale is then

$$L_d = \langle d(z)^2 \rangle^{\frac{1}{2}}, \tag{19}$$

where $d(z)$ is the distance each fluid particle has been displaced and the brackets denote vertical averaging. The minimal energy required to transform the initial profile into a stable profile (energy available for generating turbulence) is then

$$P_{av} = \frac{g}{\rho_0} \langle d(z)\,(\rho_n(z) - \rho_i(z)) \rangle. \tag{20}$$

To characterize flow stability, we define a Richardson number

$$Ri = N^2 / \langle (\partial u/\partial z)^2 \rangle. \tag{21}$$

(Note that this is a microscale quantity.) Next we introduce the Froude number which measures the relative importance of the inertial frequency and N. This is defined using the vertical integral scale L_v and the horizontal velocity

$$Fr = \langle u^2 \rangle^{\frac{1}{2}} / L_v N. \tag{22}$$

Run	$\bar{\Phi}_1(t_0)$	$\bar{\Phi}_2(t_0)$	$\bar{P}(t_0)$	N	ν	κ	dt
0A	0.527	0.524	,,	0	0.005	0.005	0.01
0B	0.527	0	,,	0	0.005	0.005	0.01
1A	0.527	0.524	0.050	0.98	0.005	0.005	0.01
1B	0.527	0	0	0.98	0.005	0.005	0.01
2A	0.527	0.524	0	2π	0.005	0.005	0.01
2B	0.527	0	0	2π	0.005	0.005	0.01
2C	0	0.524	0	2π	0.005	0.005	0.01
3A	0.527	0.524	0	4π	0.005	0.005	0.005
3B	0.527	0	0	4π	0.005	0.005	0.005
4A	0.527	0.524	0	20π	0.005	0.005	0.001
4B	0.527	0	0	20π	0.005	0.005	0.001

TABLE 1. Parameters for the numerical experiments. For these runs, $t_0 = 0.685$

3. Numerical experiments

To solve (1)–(3), we use a pseudospectral numerical code (collocation method). For time discretization we use the leap-frog scheme (stabilized by periodic averaging) with a Crank–Nicholson treatment of viscous and conductive terms. Boundary conditions are periodic in the three directions: all scales of motion are explicitly calculated. This procedure has been extensively described by Orszag & Patterson (1972) and by RMW. We simulate the flow in a 64^3 periodic cubic box, which allows $R_\lambda \leqslant 45$, with R_λ the Taylor-microscale Reynolds number. Aliasing is handled by a spherical truncation in Fourier space of the computed fields at every time step with the '2/3' algorithm described by Patterson & Orszag (1971). The leap-frog averaging period is every 50 time steps.

To initialize our runs, we follow the Orszag & Patterson (1972) procedure of generating $(u(\boldsymbol{x},0), v(\boldsymbol{x},0), w(\boldsymbol{x},0))$ as uncorrelated Gaussian data with prescribed spectra. For each Cartesian component, the spectrum is

$$E(k) = Ck^4 \exp(-2(k/k_\mathrm{I})^2), \tag{23}$$

where $k_\mathrm{I} = 4.760$ (peak in the spectrum), and C is such that $\langle u^2 \rangle = \langle v^2 \rangle = \langle w^2 \rangle = 1$. Incompressibility is then imposed on u, v, w. In order to match the experimental initial conditions, we first generate a three-dimensional isotropic turbulent field by running a non-buoyant calculation until $t_0 = 0.685$ (the time unit is the initial turnover time of the largest simulated structures) and then switching on the buoyancy to the experimental value. (The time t_0 allows the initially Gaussian $\boldsymbol{u}$ to develop into a non-Gaussian field, typical of decaying turbulence.) The resulting velocity field is the initial field for all runs in this paper. The parameters of this and subsequent runs are described in table 1.

3.1. *Comparisons with laboratory experiments*

To validate our numerical techniques, we chose the Brunt–Väisälä frequency N, and the initial perturbation density field $\Theta(\boldsymbol{x})$ in such a way that the initial values of kinetic energy, potential energy, and buoyancy flux $\langle \Theta w \rangle$ are in the same ratio as in the laboratory experiment of Itsweire *et al.* (1986). The experiment with which we compare our simulation is freely evolving, unsheared, grid-generated turbulence in a ten-layer, closed-loop, salt-stratified water channel. An important difference between our simulations and the experiments is that the experimental Prandtl number is of

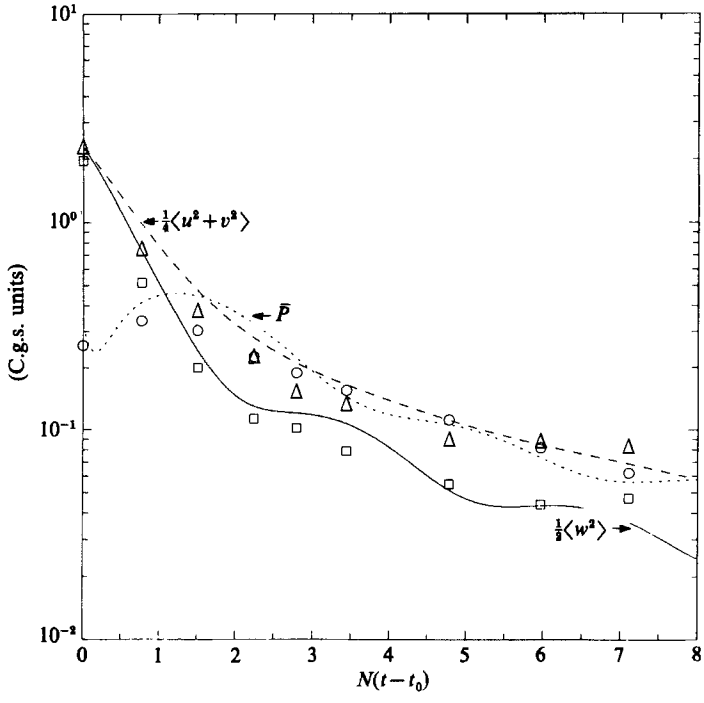

FIGURE 2. Time evolution of half the horizontal kinetic energy $\frac{1}{4}(\langle u^2\rangle+\langle v^2\rangle)$ (– – –), vertical kinetic energy $\frac{1}{2}\langle w^2\rangle$ (——), and total potential energy $\bar{P}(t)$ (· · · · ·) for run 1A (see table 1). The time is normalized by the Brunt–Väisälä frequency ($N = 0.98$). t_0 is the time at which the stratification is turned on. △, □, and ○ are the corresponding evolutions obtained in the laboratory experiment by Itsweire *et al.* (1986).

the order of 200 in salt water. This value is inaccessible numerically with the current resolutions. Our position here is that the computational Prandtl number of order unity may perhaps give the same large-scale structures as a very high experimental value, since the large scales are determined by an effective eddy Prandtl number close to unity (actually ≈ 0.6; cf. Lesieur 1987). Another difference is that, behind the grid, $R_\lambda \approx 60$ while $R_\lambda(t_0) \approx 40$ in the computations. We choose $N = 0.98$, so that $Fr(t_0) = 2.5$ and $Ri(t_0) = 0.01$. Other run parameters are shown in table 1.

In figures 2, 3 and 4 the time is normalized by N. Figure 2 compares direct numerical simulations to the laboratory experiments of Itsweire *et al.* (1986). We show the time evolution of half the horizontal kinetic energy, $\frac{1}{4}(\langle u^2\rangle+\langle v^2\rangle)$, vertical kinetic energy, $\frac{1}{2}\langle w^2\rangle$, and total potential energy $\bar{P}(t)$. The numerical results show initially the vertical kinetic energy to be strongly damped by the stratification. Subsequently, it exhibits a periodic exchange with potential energy, with period πN^{-1}. The horizontal kinetic energy does not exhibit any oscillations. Except for the initial growth of potential energy (which seems to be numerically overestimated), agreement with the experiment is good: the discrepancies do not exceed $\approx 20\%$ after the initial phase.

The numerical simulations presented here are of course subject to uncertainties, as are the actual experiments of Itsweire *et al.* (1986). Of particular concern is the question of whether the combined errors between numerical simulations and experiments may accidentally induce a closer agreement. Although we have no direct data on this point, we conclude that this is not the case. First, the numerical errors

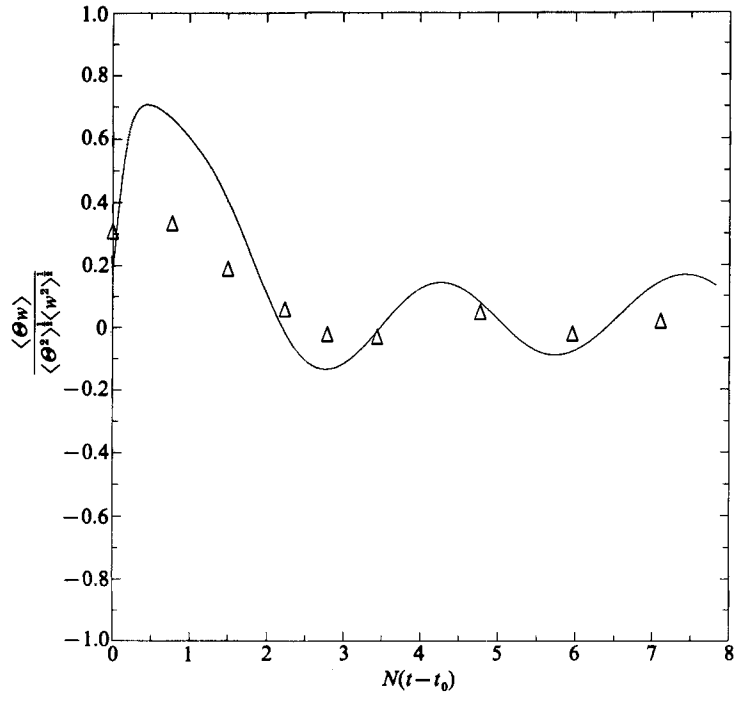

FIGURE 3. Time evolution (normalized by N) of the normalized buoyancy flux $\langle \Theta w \rangle / \langle \Theta^2 \rangle^{\frac{1}{2}} \langle w^2 \rangle^{\frac{1}{2}}$ for run 1A compared to the experimental values by Itsweire *et al.* (1986) (△).

bars are smaller than those reported by Schumann & Herring (1976) (since the present resolution is twice theirs). The errors in the experiments are estimated as about 12% (E. C. Itsweire, private communication), whereas those in the Schuman–Herring simulation are smaller (about 5%); thus the overlap of errors is not sufficient to explain the discrepancy between simulations and experiments.

The time evolution of the normalized buoyancy flux $\langle \Theta w \rangle / (\langle \Theta^2 \rangle^{\frac{1}{2}} \langle w^2 \rangle^{\frac{1}{2}})$ is plotted in figure 3. The computed flux undergoes a much stronger initial build up than that of the experiment. Then in both cases, because of internal wave, the flux exhibits periodic oscillations around zero (period $\approx \pi N^{-1}$). These are much more strongly damped in the salt-stratified experiment, but recent stratified wind-tunnel grid-turbulence experiments performed by Lienhard (1988) show oscillations closer to the amplitude of the numerical simulations, suggesting that the stronger damping is attributable to Prandtl-number differences.

In figure 4, we plot the time evolution of the lengthscales L_K, L_R, L_b, L_t, as previously defined. The numerical L_t exhibits a value at its maximum larger than the experimental, as previously noticed for the potential energy. The experimental Kolmogorov scale is half as large as the numerical one, but both seem to follow a linear law with respect to $N(t-t_0)$. An extensive discussion of the evolution of these scales has been given by Gibson (1980), Dillon (1982), Stillinger *et al.* (1983), and Itsweire *et al.* (1986).

Having seen the extent to which direct numerical simulation reproduces the experimental results, we next allowed the flow to decay for longer than in the experimental channel (which is limited by experimental accuracy) and examine various statistical quantities that are experimentally inaccessible.

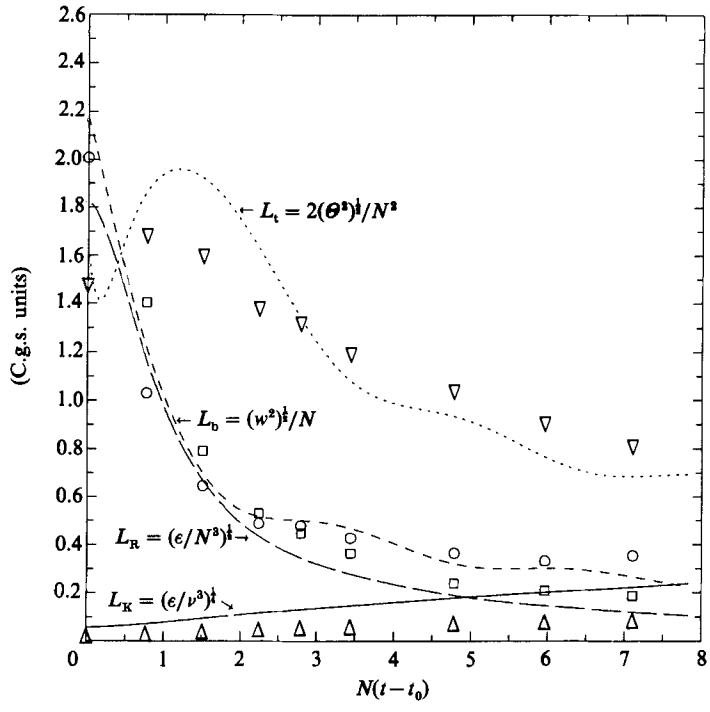

FIGURE 4. Time evolution (normalized by N) of the length scales L_R (———), L_b (– – –), L_t (· · · · ·), and L_K (——) (see (14), (15), (16), (17)) for run 1A. □, ○, ▽, and △ are the experimental points extracted from Itsweire *et al.* (1986).

3.2. *Turbulence collapse*

Parallel to the preceding calculation (run 1A) where the initial conditions ($t = t_0$) were isotropic, we have carried out another calculation (run 1B) with the velocity field projected at $t = t_0$ onto the vector $\boldsymbol{e}_1$ (such that $\bar{\Phi}_2(t_0) = 0$). Furthermore, for this second case, we took the potential energy $\bar{P}(t_0) = 0$. Runs 0A and 0B parallel runs 1A and 1B, but for the non-buoyant case ($N = 0$).

Note that the above projection must, to a certain extent, affect the intermodal transfer, thereby temporarily decreasing higher-order measures of transfer such as kurtosis and skewness. However, our pimary goal here is to explore the effects of initial conditions on the late time characteristics for the flow. Our experiments (itemized in table 1) are thus designed to give a set of independent initial conditions rather than to represent fully evolved decaying turbulence.

3.2.1. *Energetics*

Figures 5(*a*) and 5(*b*) show $\bar{\Phi}_1(t)$ ('vortex' kinetic energy) in the stratified case ($N = 0.98$, runs 1A and 1B) compared to the non-buoyant case ($N = 0$, runs 0A and 0B), $\bar{\Phi}_2(t)$ ('wave' kinetic energy), and $\bar{P}(t)$ (potential energy) for runs 1A and 1B. (We recall that the time unit is the initial turnover time of the largest simulated structures.) The wave kinetic energy exhibits a periodic exchange with the potential energy, whose period is $\approx \pi N^{-1}$, and, in the mean, the internal wave energy, as one could expect (Gill 1982), is equally divided between the kinetic and potential forms. In case B, the wave kinetic energy and potential energy, initially zero, increase until they are equipartitioned. Then, both are dissipated at the same rate and exhibit

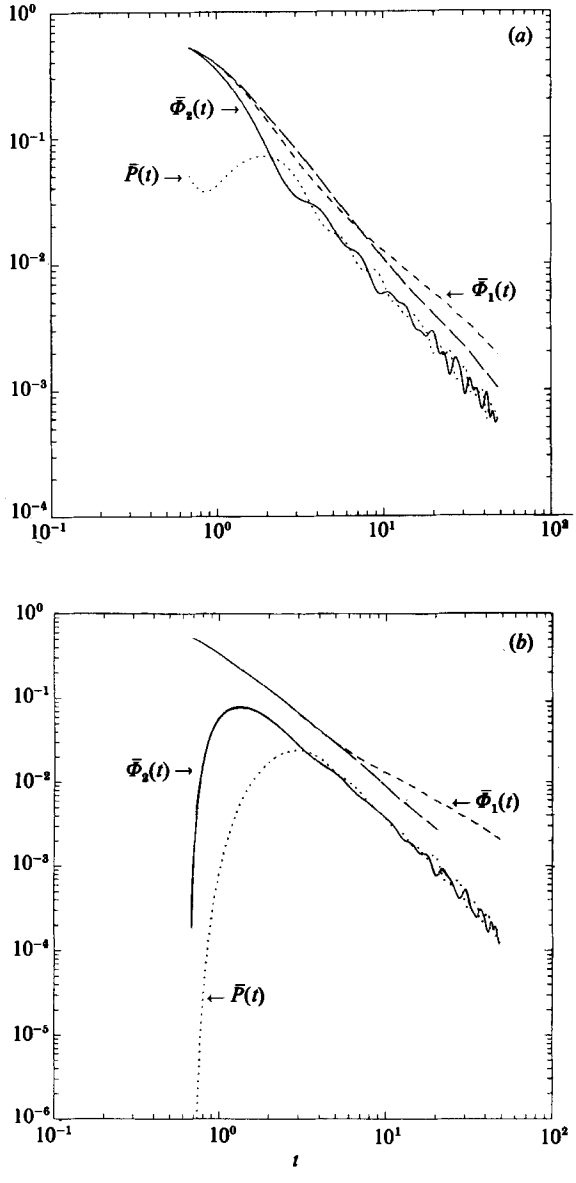

FIGURE 5. (*a*) Time evolution of the 'vortex' kinetic energy $\bar{\Phi}_1$ (– – – –) in the stratified case ($N = 0.98$, run 1A) compared to $\bar{\Phi}_1$ (— — —) obtained in a non-buoyant calculation with the same initial conditions ($N = 0$, run 0A), 'wave' kinetic energy $\bar{\Phi}_2$ (——, run 1A), and potential energy $\bar{P}$ (· · · · ·, run 1A). The time unit is the turnover time at $t = 0$ of the largest simulated structures. The initial turbulent velocity field is three-dimensional isotropic: $\bar{\Phi}_1(t_0) = \bar{\Phi}_2(t_0)$. (*b*) Same as (*a*) for runs 1B and 0B: $\bar{\Phi}_1(t_0)$ is the same as (*a*), but $\bar{\Phi}_2(t_0) = 0$ (vortical initial conditions).

oscillations with amplitude severely reduced from those in the previous case. In both cases, vortex kinetic energy does not exhibit oscillations, suggesting weak interactions between wave and turbulence components. The vortex kinetic energy decay does not seem to be affected by the stratification at the beginning of the evolution. The decay law is initially approximately $t^{-1.56}$. An extensive discussion of these decay laws in the case of isotropic turbulence for the kinetic energy and the

passive-scalar variance (equivalent to the potential energy in the non-buoyant case) has been given by Herring *et al.* (1982). After the initial decay phase, a clear slow-down is observed in the decay rate for $t_c \geqslant 6N^{-1}$, which could be the indication of a turbulence 'collapse' at time t_c, $Fr \approx 0.27$ and $Ri \approx 2$. The moving-grid experiment of Dickey & Mellor (1980) showed a similar clear break in the decay rate of the turbulence energy at an identical time and close to the present value of the Froude number. In case A, the wave energy (wave kinetic energy + potential energy) remains roughly equipartitioned (within statistical scatter) with vortex kinetic energy throughout the decay; the proportion of vortex kinetic energy does not exceed 60% of the total energy. In case B, the energy is at first equally partitioned between wave and vortex components of energy. After the transition, the proportion of vortex kinetic energy increases, reaching 87% at the end of the run. These calculations illustrate the lack of universality and a dependence on the initial conditions of stratified turbulence. We return to this point in more detail in §3.3, when discussing the very low-Froude-number regime.

3.2.2. *Lengthscales and Froude number*

Figure 6(*a*), (*b*) shows the time evolution of the Kolmogorov scale L_K, the Ozmidov scale L_R, the horizontal integral scale L_h, the vertical integral scale L_v, and the Thorpe scale L_d for runs 1A and 1B. The collapse time seems to coincide with the time at which the Ozmidov and Kolmogorov scales are equal; i.e. all the turbulent scales are influenced by buoyancy. From the beginning of the decay ($Fr \approx 1$), stratification enhances the growth of the horizontal integral scale as noticed by RMW. The vertical integral scale seems to be frozen by the stratification and varies only slightly around its initial value until it is caught by the Kolmogorov scale; afterwards they remain comparable. The Thorpe scale catches up with the Ozmidov scale and then decays at the same rate. At the time of collapse, when vertical overturning no longer occurs, the Thorpe scale decreases much more rapidly. When L_d reaches its maximum, the energy P_{av} (see (20)) is only 33% of the potential energy in case A and 16% in case B.

The course of $Fr(t)$ for runs 1A and 1B is shown in figure 7. For both runs, the initial $Fr \approx 1$, and for both cases, $Fr(t)$ evolves similarly ($Fr \approx 0.07$ at large t). It is possible that the small pulse here in 1A at $t \sim 5$ is an indicator of the collapse noted above. In this connection, we should note that the collapse could be signalled by a temporary increase of Fr, since (according to (22)) such an event may occur with a sharp decrease of L_v (see (13)), with $\langle u^2 \rangle$ remaining smooth. Runs at larger N evolve towards lower values of Fr, but with $Fr(t)$ decreasing more strongly with t (as $t \to \infty$) than shown in figure 7. Also at larger N, $Fr(t)$ tends to execute a damped oscillation as a function of t.

3.2.3. *Energy and transfer spectra*

In figure 8, we present horizontal two-dimensional spectra $\Phi_1(K_h)$ for the buoyant ($N = 0.98$, run 1A) and non-buoyant case ($N = 0$, run 0A), $\Phi_2(K_h)$ (run 1A), and $P(K_h)$ (run 1A) at $t = 3.88$. K_h is the horizontal wavenumber

$$K_h = (k_x^2 + k_y^2)^{\frac{1}{2}}. \tag{24}$$

$\Phi_1(K_h)$ is the only non-zero spectrum for purely two-dimensional turbulence. The wave kinetic energy and potential energy are in rough equipartition throughout the wavenumber domain. However, the relative positions of $P(K_h)$ and $\Phi_2(K_h)$ are changed if the energy is plotted at a different phase of the Brunt–Väisälä period. For

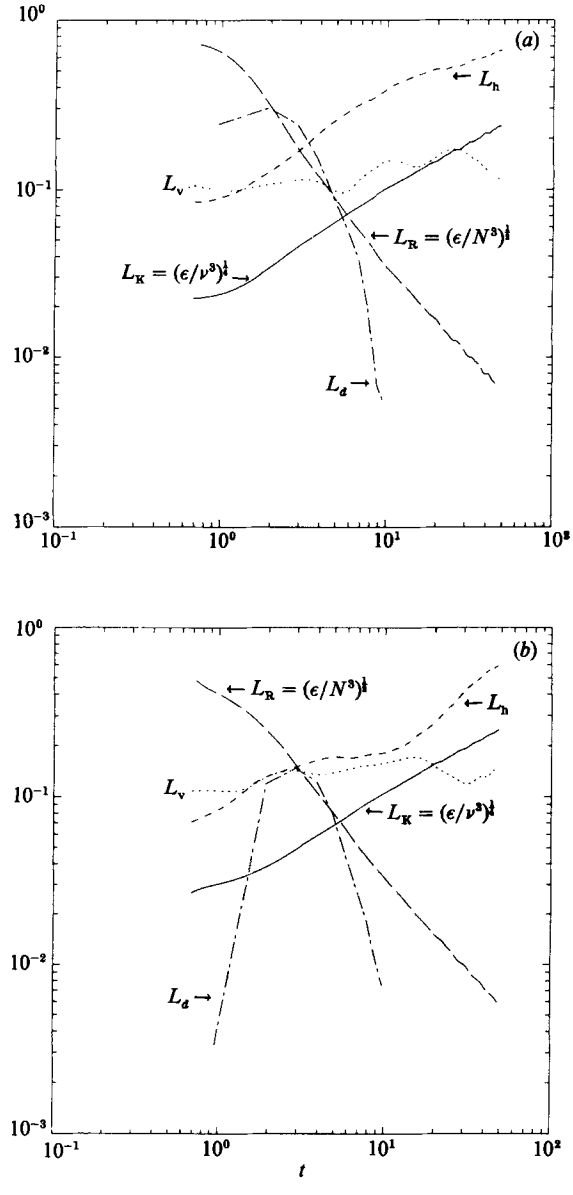

FIGURE 6. (*a*) Time evolution of the Kolmogorov scale L_K (——), the Ozmidov scale L_R (— — —), the horizontal integral scale L_h (– – –) defined by (12), the vertical integral scale L_v (· · · · ·) defined by (13) and the Thorpe scale (—·—·) defined by (19) for run 1A. (*b*) Same as (*a*) for run 1B.

the stratified case (run 1A), the vortex component dominates the large scales and the wave component the small scales. As mentioned by RMW, stratification seems to inhibit the spectral transfer of energy towards small scales, leaving less energy in the latter, increasing the vortex component slope in the inertial range, and inducing a weaker horizontal dissipation of this component. The stratification enhances the growth of the vortex-kinetic-energy largest scales. Furthermore, a comparison of the horizontal and vertical one-dimensional spectral distributions shows that each component dissipates its energy by vertical variability; in the dissipative range, $E(k_z) \gg E(k_y)$; $E = \Phi_1, \Phi_2$ or P.

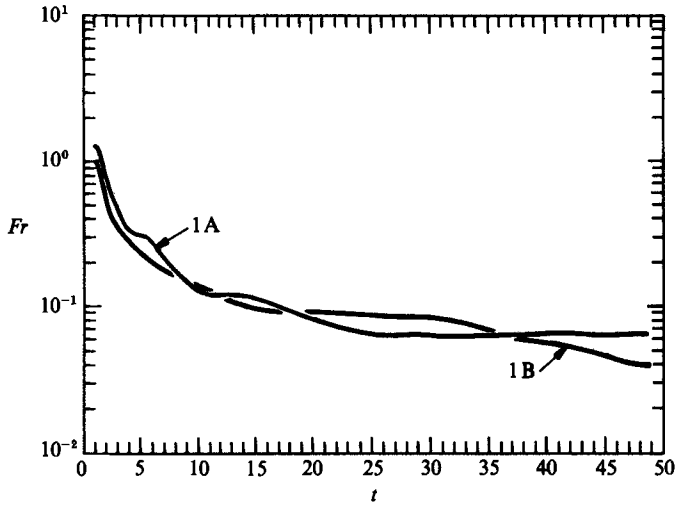

FIGURE 7. Froude number (see (22)) as a function of time for runs 1A (isotropic initial conditions), and 1B (vortex initial conditions). Timescale is the same as in figure 6.

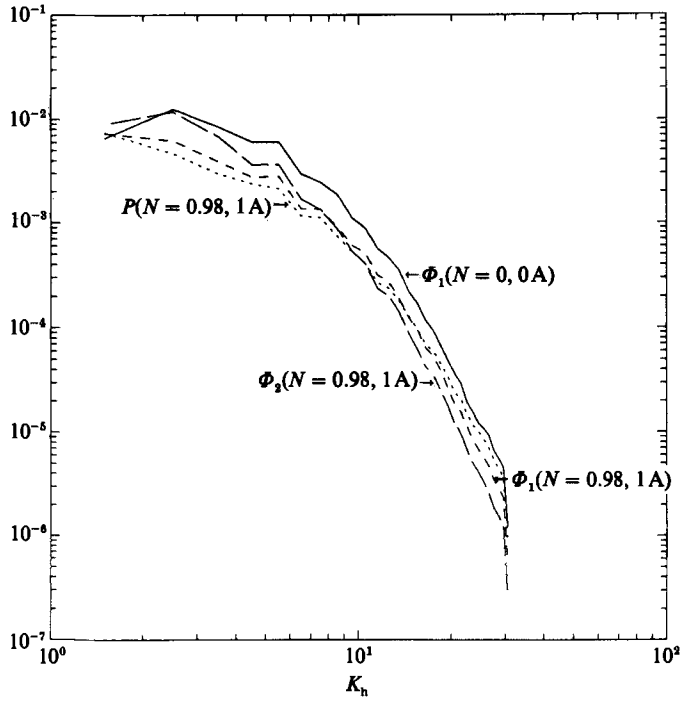

FIGURE 8. ——, horizontal two-dimensional spectra $\Phi_1(K_h)$, non-buoyant case ($N = 0$, run 0A); — — —, buoyant case ($N = 0.98$, run 1A); – – –, $\Phi_2(K_h)$ (run 1A); · · · · ·, $P(K_h)$ (run 1A). All at 3.88. $K_h = (k_x^2 + k_y^2)^{\frac{1}{2}}$, k_x and k_y are the horizontal wave vector components.

We next examine energy transfer spectra which give the time rate of change of energy spectra due to nonlinear interactions

$$\left(\frac{\partial}{\partial t}+2\nu k^2\right)\Phi_1(\boldsymbol{k},t)=\mathscr{T}_1(\boldsymbol{k},t), \tag{25}$$

where the transfer function, $\mathscr{T}_1(\boldsymbol{k},t)$, corresponds to triple correlations coming from the nonlinear terms of (1). Similar equations can be derived for $\Phi_2(\boldsymbol{k},t)$ and $P(\boldsymbol{k},t)$, but these involve spectral covariances of ϕ_2–Θ in addition to triple correlations. For the latter, we need the quantity,

$$\hat{V}(\boldsymbol{k},t)=\langle\hat{\phi}_2(-\boldsymbol{k},t)\,\hat{\Theta}(\boldsymbol{k},t)\rangle. \tag{26}$$

$\mathscr{T}_1$ involves $\langle\hat{\phi}_1\hat{\phi}_1\hat{\phi}_1\rangle$, $\langle\hat{\phi}_1\hat{\phi}_2\hat{\phi}_1\rangle$, and $\langle\hat{\phi}_1\hat{\phi}_2\hat{\phi}_2\rangle$ terms, which correspond respectively to contributions due to vortex–vortex (vv), vortex–wave (vw), and wave–wave (ww) interactions. The formulation of these various interactions has been given by Riley (1985). We may then write

$$\mathscr{T}_1=\mathscr{T}^{\mathrm{v}}_{\mathrm{vv}}+\mathscr{T}^{\mathrm{v}}_{\mathrm{wv}}+\mathscr{T}^{\mathrm{v}}_{\mathrm{ww}}. \tag{27}$$

The transfer function, $\mathscr{T}_2(\boldsymbol{k},t)$ in the equation of evolution of $\Phi_2(\boldsymbol{k},t)$, can be decomposed in a similar way:

$$\mathscr{T}_2=\mathscr{T}^{\mathrm{w}}_{\mathrm{ww}}+\mathscr{T}^{\mathrm{w}}_{\mathrm{vw}}+\mathscr{T}^{\mathrm{w}}_{\mathrm{vv}}. \tag{28}$$

The following conservation properties can be analytically checked:

$$\int_0^\infty \mathscr{T}^{\mathrm{v}}_{\mathrm{vv}}(k)\,\mathrm{d}k=\int_0^\infty \mathscr{T}^{\mathrm{w}}_{\mathrm{ww}}(k)\,\mathrm{d}k=0. \tag{29}$$

In the following discussion, $E(k)$ stands for an isotropically accumulated spectrum and $E(K_{\mathrm{h}})$ for a horizontal spectrum of $E(\boldsymbol{k})$ (cf. RMW). The components of $\mathscr{T}_1(k)$ as given by (27) are shown in figure 9(a, b) at $t=8.76$, for the non-buoyant case ($N=0$, run 0A), and for the buoyant case ($N=0.98$, run 1A). We note the inhibition by the stratification of the spectral transfer towards small scales, confining the major part of the transfer to the smaller wavenumbers. Furthermore, the stratification reduces the amplitude of the contributions vwv and vww and changes the vww sign in the largest scales. The collapse is accompanied by a significant change of the vortex–vortex-interactions contribution compared to the isotropic case; after t_{c}, vvv is enhanced by the stratification and becomes dominant. This remark applies also to the vvv contribution to $\mathscr{T}_1(k_z)$ (k_z = vertical wavenumber) (see figure 10a, b).

By contrast, the contribution of vortex–vortex interaction to $\mathscr{T}_1(K_{\mathrm{h}})$ (figure 11a, b) has similar amplitude in the buoyant and non-buoyant cases. This strictly two-dimensional term resembles a two-dimensional energy transfer function, positive in the large energy-containing eddies (back transfer), similar to the one calculated by Herring *et al.* (1974). However, this resemblance is also true in the case of three-dimensional isotropic turbulence (cf. RMW). Furthermore, in vwv, the wave–vortex interaction strongly drains the stratified turbulence in the largest horizontal scales.

3.2.4. *Spatial structures of the three-dimensional field*

Figure 12(a–f), isosurfaces of the total density field $\bar{\rho}(z)+\rho'(x,y,z,t)$, shows the spatial structure of the flow from $t=2.91$ to 7.78, and illustrates the collapse. For the earlier time, we note complicated three-dimensional convoluting of the isosurface. At

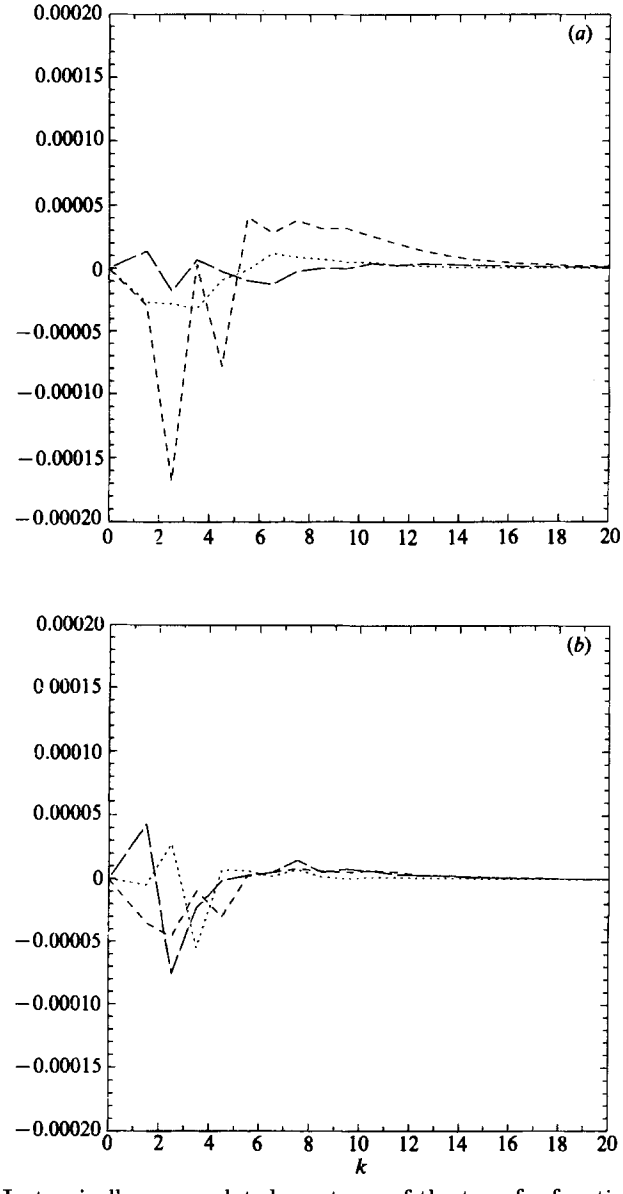

FIGURE 9. (*a*) Isotropically accumulated spectrum of the transfer function $\mathscr{T}_1$ (see (25), (27)) for run 0A. Here $t = 8.76$. ———, the contribution due to vortex–vortex interactions ($\mathscr{T}^{\mathrm{v}}_{\mathrm{vv}}$); – – – –, the contribution due to vortex–wave interaction ($\mathscr{T}^{\mathrm{v}}_{\mathrm{wv}}$); · · · · ·, contribution due to wave–wave interaction ($\mathscr{T}^{\mathrm{v}}_{\mathrm{ww}}$). (*b*) Same as (*a*) for run 1A.

the time of collapse, the convolutions suddenly disappear. This corresponds to the break in the Thorpe-scale curve observed in figure 6(*a*). From place to place, very sharp peaks signal strong wave–wave interactions. After the collapse, the flow is convectively stable everywhere, although some sharp peaks remain.

3.3. *Small-Froude-number regime*

We next examine a very small-Froude-number regime in order to understand possible universal aspects of the flow. We discuss three runs: the first examines the

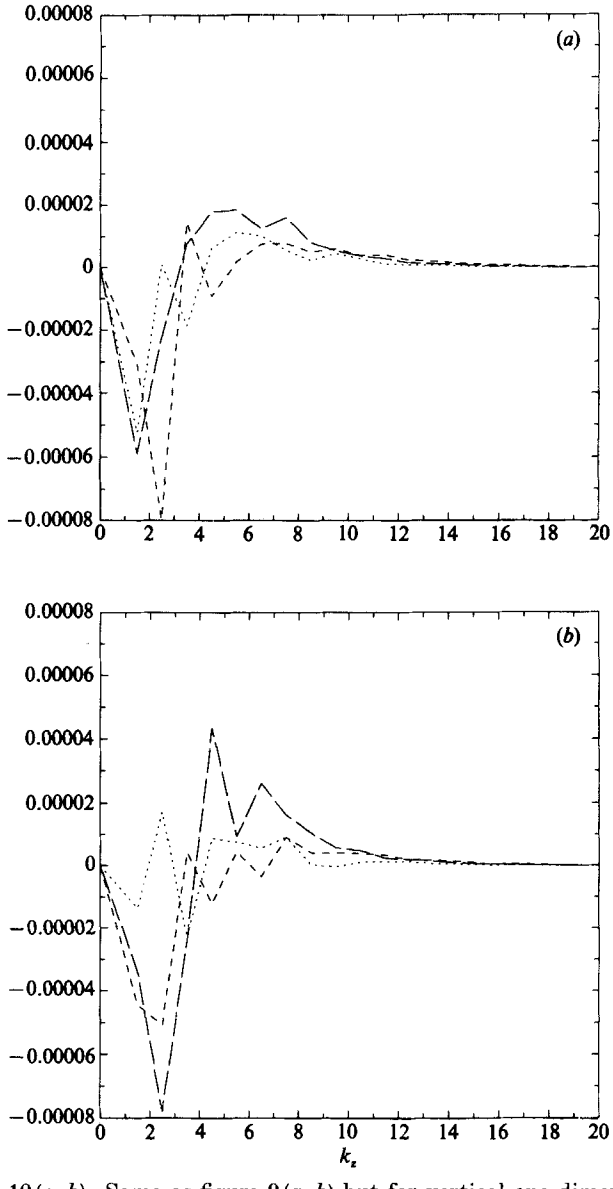

FIGURE 10(*a*, *b*). Same as figure 9(*a*, *b*) but for vertical one-dimensional spectra.

issue of equipartitioning between waves and turbulence (case A); the second examines the extent to which two-dimensional turbulence survives as $Fr \to 0$ (case B); and in the third the system is initially entirely waves (case C). In all these cases, we vary the Brunt–Väisälä frequency to assess the dependence of the flow on this parameter. We could also examine the balance of initial conditions or introduce a wave damping in order to study vortical turbulence. However, in this case, as numerical calculations suggest, the wave component tends to zero as $N \to \infty$, so such refinements may not be necessary in the limit of large N.

Runs 2A, 3A, and 4A parallel runs 0A and 1A for three values of $N = (2\pi, 4\pi, 20\pi)$, except that the initial potential energy is taken equal to zero. According to Hunt, Stretch & Britter (1988), the absence of initial density fluctuations increases the

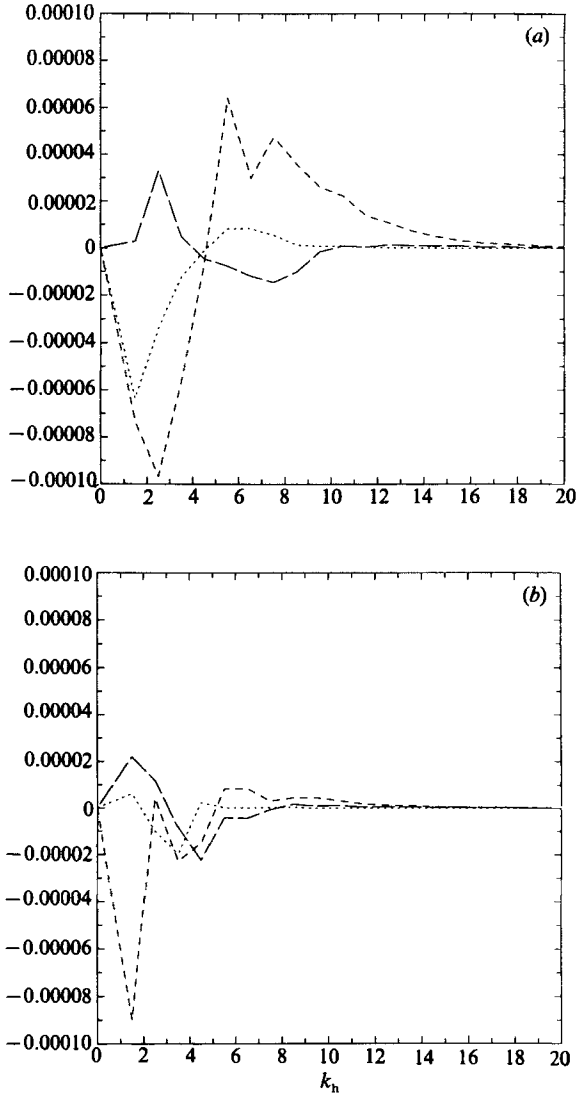

FIGURE 11 (*a*, *b*). Same as figure 9 (*a*, *b*) but for horizontal two-dimensional spectra.

initial oscillations in the potential energy and wave kinetic energy. However, we are interested here in long-term evolutions for which these zero initial conditions have no consequences according to our numerical studies. The initial Froude numbers are respectively 0.2, 0.1, and 0.02; the other runs parameters are given in table 1. $\bar{\Phi}_1(t)$, $\bar{\Phi}_2(t)$, and $\bar{P}(t)$ are shown in figure 13 for run 2A. These evolutions are similar to those observed in run 1A. Despite the strong oscillatory behaviour of the wave kinetic energy, the vortex kinetic energy does not exhibit any oscillations, a sign of weak interactions between the two components. Also, we may surmise that Φ_1 correctly identifies the non-wave component of the dynamics. Note that, starting from $\bar{\Phi}_1(t_0) = \bar{\Phi}_2(t_0), \bar{P}(t_0) = 0$, the system does not approach the symmetry of thermal equilibrium ($\bar{\Phi}_1 = \bar{\Phi}_2 = \bar{P}$), but the energy remains equally divided between the vortex kinetic energy and the total wave energy (wave kinetic + potential energy). The equipartition between the two forms of energy is preserved when the

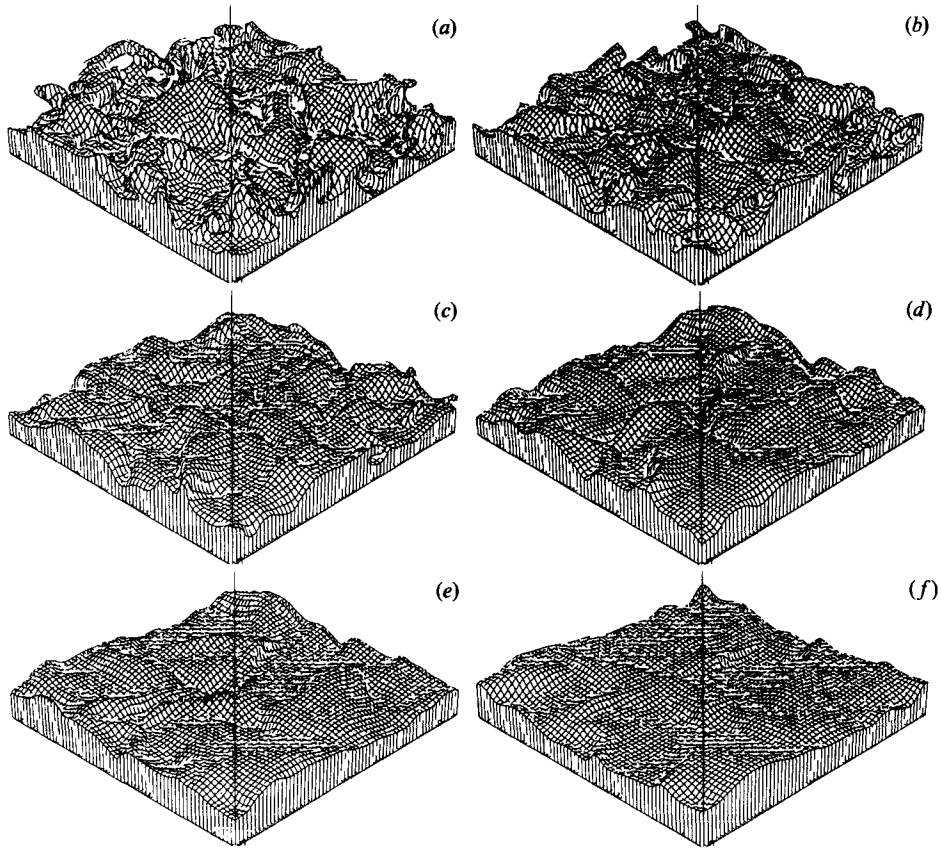

FIGURE 12. Isosurfaces of the total density field $\bar{\rho}(z)+\rho'(x,y,z,t)$ for run 1A: (*a*) $t = 2.91$; (*b*) 3.88; (*c*) 4.86; (*d*) 5.84; (*e*) 6.81; (*f*) 7.79.

stratification is increased, and the total energy dissipation decreases with increasing stratification. However, the flow remains strongly dissipative.

The equipartitioning noted above is a global property and does not hold in spectral detail. There is an excess of Φ_1 at large K_h and a deficit at small K_h. The converse holds for k_z, with rough equipartitioning in the isotropic k energy-containing range.

The weak interactions between waves and turbulence components is confirmed in figure 14(*a*, *b*). This shows $\mathscr{T}_1(K_h)$ and $\mathscr{T}_1(k_z)$ for run 4A, at $t = 3.93$. The horizontal and vertical transfer functions of vortical energy are both dominated by the vortex–vortex interaction contributions. $\mathscr{T}^v_{vv}(K_h)$ is concentrated in the very large scales, and is similar to a strictly two-dimensional transfer function. However, $\mathscr{T}^v_{vv}(k_z)$ is not small, and resembles a three-dimensional transfer function; it is negative in the large energy-containing eddies, and positive at higher wave numbers, indicating an energy cascade from large to small vertical dissipative scales.

We next examine, in case B, $\bar{\Phi}_1(t_0) \neq 0, \bar{\Phi}_2(t_0) = \bar{P}(t_0) = 0$, and a three-dimensional distribution for Φ_1. Runs 2B, 3B, and 4B correspond to $N = (2\pi, 4\pi, 20\pi)$. In figure 15, we plot $\bar{\Phi}_1(t), \bar{\Phi}_2(t)$ and $\bar{P}(t)$ for run 2B. After a transient phase in which $\bar{\Phi}_2$ and $\bar{P}$ increase from zero, $\bar{\Phi}_1$ tends to dominate. Part of ϕ_2 observed here may be genuine gravity waves, and part may correspond to 'vortical' motions on a surface whose normal defines that component of vorticity conserved in Ertel's theorem; we have

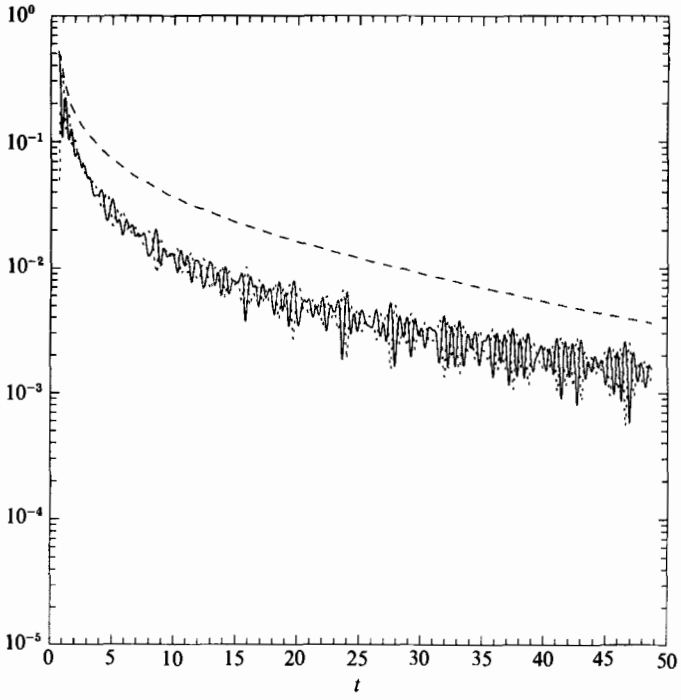

FIGURE 13. $\bar{\Phi}_1(t)$ (– – – –), $\bar{\Phi}_2(t)$ (——), and $\bar{P}(t)$ (· · · · ·) for run 2A ($N = 2\pi$, isotropic initial conditions).

here no tools to distinguish between these alternatives. The wave kinetic energy and potential energy exhibit parallel evolution, but during the initial transient phase the latter exceeds more and more the former as the stratification increases. This could indicate that during this initial phase, $\bar{\Phi}_2$ created by the initial vortices does not correspond to waves but more to small-scale three-dimensional (non-buoyant) turbulence.

In figure 16, we plot the ratio $\bar{\Phi}_1/(\bar{\Phi}_1+\bar{\Phi}_2+\bar{P})$ as a function of the normalized time $N(t-t_0)$. After an adjustment phase (of the order of $0.8N^{-1}$) during which the ratio decreases, the initial vortex motion remains dominant over the gravity-wave component at subsequent time, and the relative amplitude of the gravity-wave component decreases with increasing stratification. The flow becomes less dissipative with increasing N. However, although dominated by horizontal motion, it is not characterized by weak energy dissipation, as in two-dimensional turbulence.

Figure 17 (a, b) is the analogue of figure 14 (a, b) for run 4B. The contributions of the vortex–wave and wave–wave interactions to $\mathscr{T}_1(K_h)$ and $\mathscr{T}_1(k_z)$ tend to zero as the stratification increases. $\mathscr{T}^{\mathrm{v}}_{\mathrm{vv}}(K_h)$ and $\mathscr{T}^{\mathrm{v}}_{\mathrm{vv}}(k_z)$ are almost identical (in both shape and intensity) for runs 4A and 4B. Because of the importance of the vertical variability, it is of interest to examine the vertical wavenumber spectra $\Phi_1(k_z)$, $\Phi_2(k_z)$ and $P(k_z)$ figure 18, run 4B, $t = 3.93$): $\Phi_1(k_z)$ dominates at all scales. The low resolution does not allow us to determine if the vortex component vertical spectrum is consistent with the 'saturated' wave-spectrum assumption scaling as $N^2k_z^{-3}$. The $P(k_z)$ spectrum is quite flat and tails off only because of diffusive effects, possibly suggesting sharp wave fronts. The comparison of the one-dimensional spectra $\Phi_1(k_z)$ and $\Phi_1(k_y)$ (figure 19, run 4B, $t = 3.93$) shows that the dissipation of the total energy is primarily attributable to the vertical variability of the vortex component.

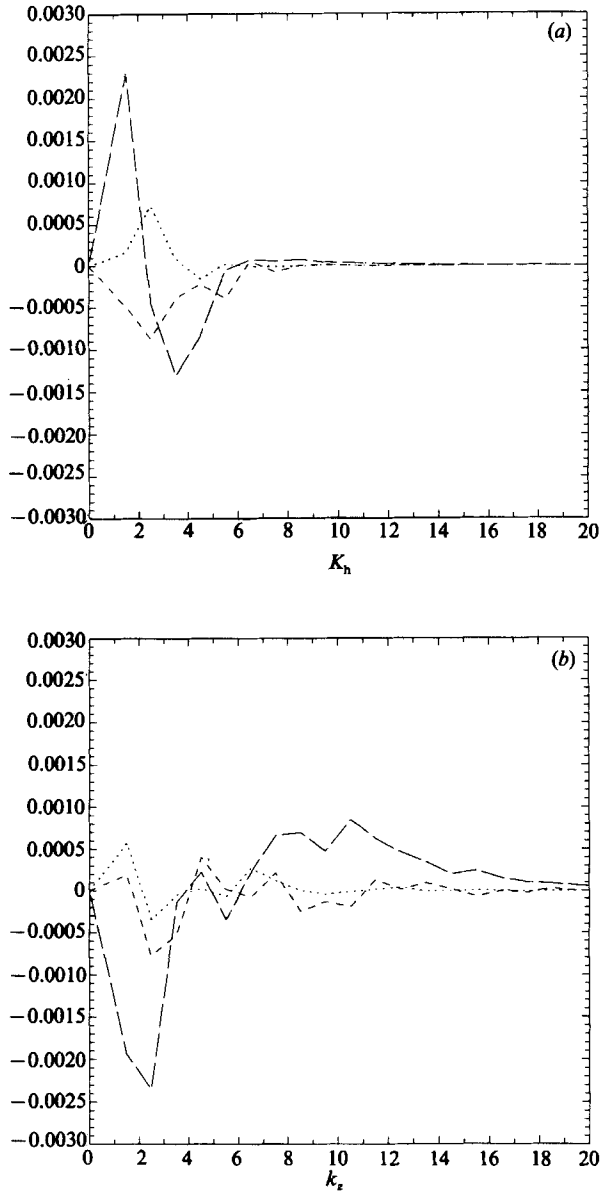

FIGURE 14. (*a*) Same as figure 11 (*a*) for run 4A. (*b*) Same as (*a*) but for vertical one-dimensional spectra (k_z, vertical wave vector component).

Run 2C parallels runs 2A and 2B ($N = 2\pi$), but with $\boldsymbol{u}(t = t_0)$ projected onto $\boldsymbol{e}_2(\bar{\Phi}_1(t_0) = 0)$. The initial density fluctuations also are taken equal to zero ($\bar{P}(t_0) = 0$). Figure 20 shows $\bar{\Phi}_1(t), \bar{\Phi}_2(t)$ and $\bar{P}(t)$. The energy remains wave dominated. The wave dominance increases at large t, just as in run 2B where the vortex dominance becomes stronger as $t \to \infty$. This result is consistent with weakly interacting waves and turbulence. The bulk decay rates (i.e. total energies) for runs 2A, 2B, and 2C (figures 13, 15, and 20) are strikingly similar.

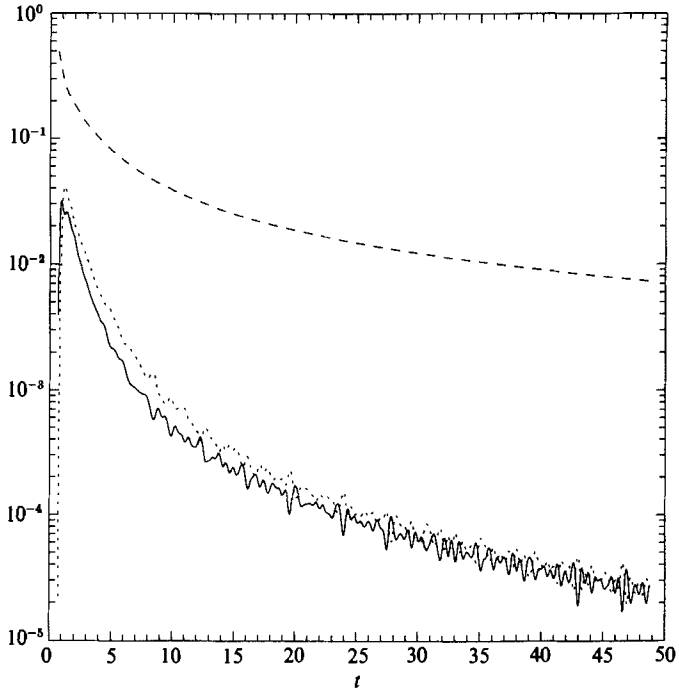

FIGURE 15. Same as figure 13, for run 2B ($N = 2\pi$, vortical initial conditions).

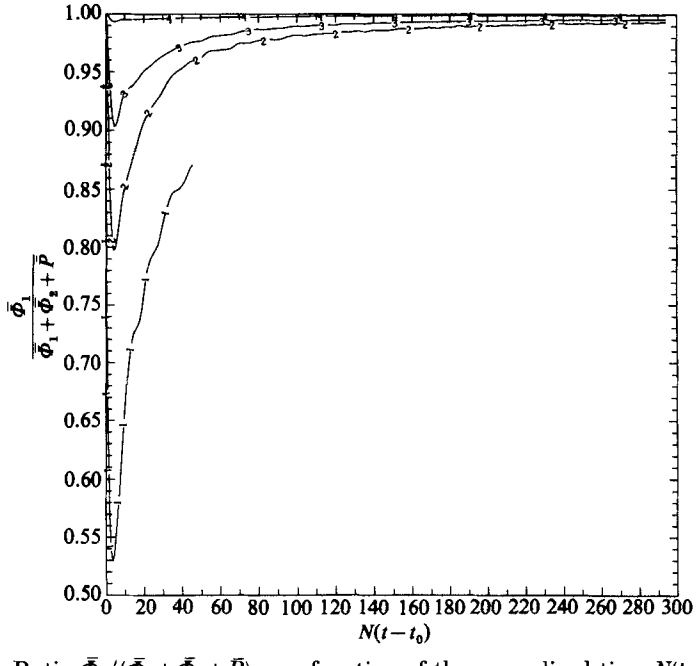

FIGURE 16. Ratio $\bar{\Phi}_1/(\bar{\Phi}_1+\bar{\Phi}_2+\bar{P})$ as a function of the normalized time $N(t-t_0)$. Vortical initial conditions: 1, run 1B ($N = 0.98$); 2, run 2B ($N = 2\pi$); 3, run 3B ($N = 4\pi$); 4, run 4B ($N = 20\pi$).

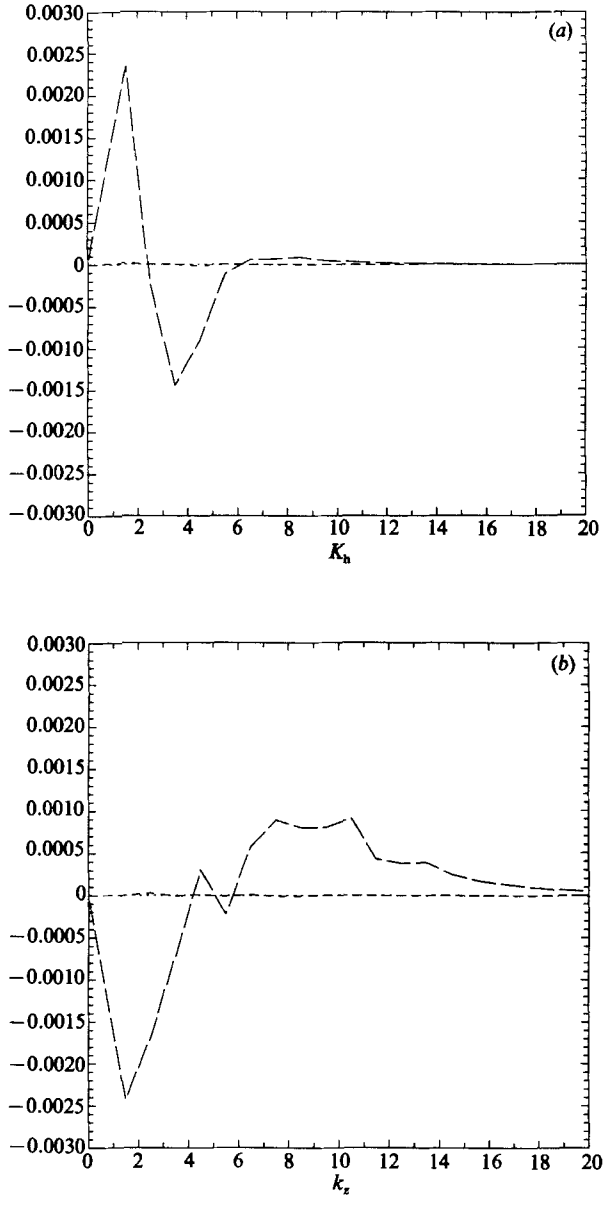

FIGURE 17 (*a*, *b*). Same as figure 14 (*a*, *b*) for run 4B.

3.3.1. *Frequency spectra*

The time series of, for example, density fluctuation are obtained at one point of the flow. They are then Fourier transformed and normalized to get potential-energy frequency spectra. Before describing detailed results, we remind the reader that the scope of our study is decaying flows for which power-spectra analysis may be suspect. The concern here is that decaying flow (whose variances are as in figure 5) are not suitable for examining power-spectral issues, for which, at least ideally, stationary conditions are required. However, we may readily establish, numerically that, for a time series of length comparable with ours, with several discrete frequencies (i.e.

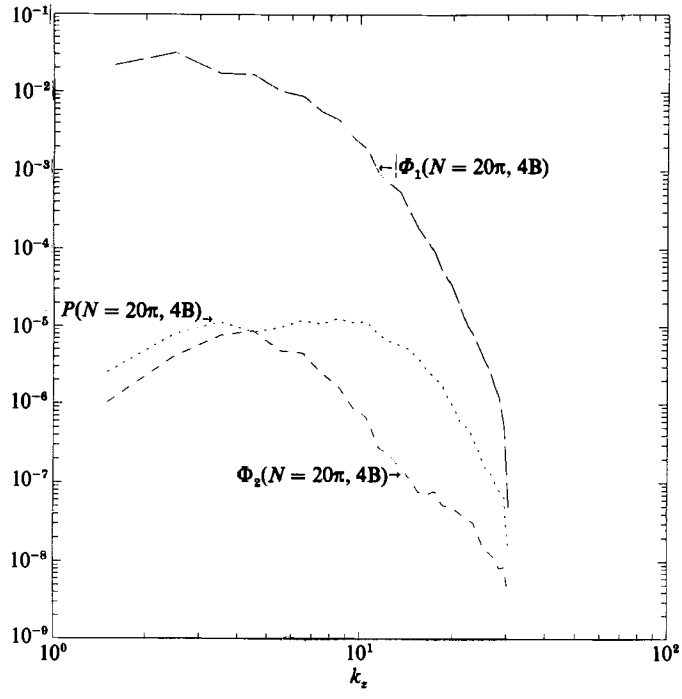

FIGURE 18. One-dimensional vertical spectra of Φ_1 (———), Φ_2 (----), and P (· · · · ·) for run 4B.

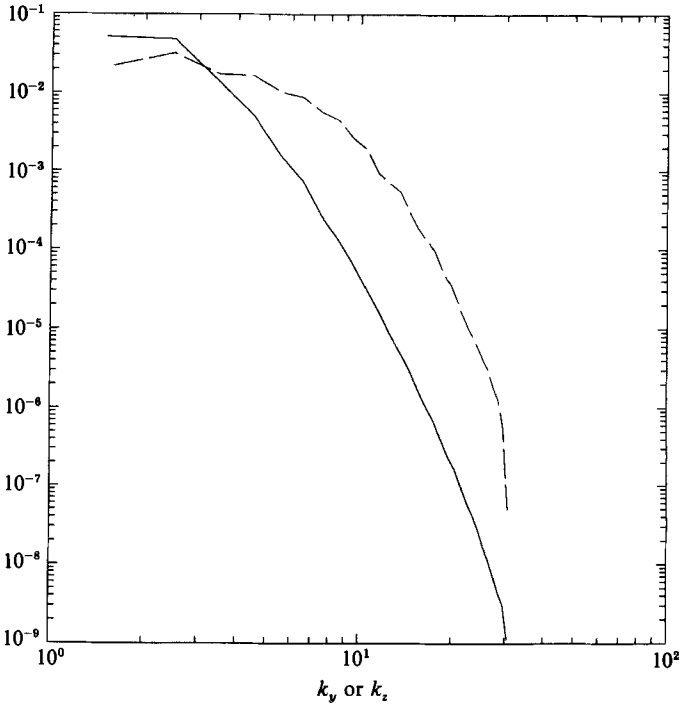

FIGURE 19. One-dimensional spectra $\Phi_1(k_y)$ (——) and $\Phi_1(k_z)$ (———) for run 4B.

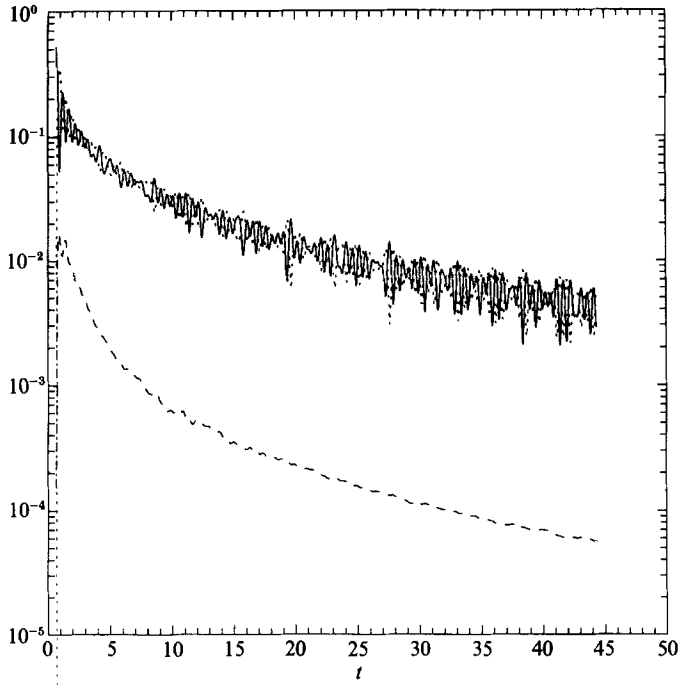

FIGURE 20. Same as for figures 13 and 15 for run 2C ($N = 2\pi$). $\Phi_2(t_0)$ is the same as run 2A, but $\Phi_1(t_0) = 0$: 'wave' initial conditions.

~ 10) and with a variance decaying as $t^{-(n\sim 1.8-2.0)}$ (see figure 5), there is no difficulty in picking out the frequencies (from the power spectra) comprising the signal. As $n \to \infty$, low-frequency power increases, but only as a continuous background.

Figure 21 (a–c) shows plots of the power spectra, $P(\omega)$ for runs 2A, 2B and 2C (ω is here the frequency normalized by N, and $N = 2\pi$). The figure shows the power spectra of the $t \geqslant 10$ part of the data, which were judged to be relatively free from the initial transient. The three spectra exhibit discrete spectral peaks extending from near the Brunt–Väisälä frequency (slightly below for run 2C) down to about $0.2N$ at the lower frequency end. The location of these peaks (there are about eight of them visible) seem to be about the same for all the runs. For $\omega \geqslant 1$, the power spectra drop abruptly. The approximately $\omega^{-2}, \omega \geqslant 1$ part of the spectra results from the finite length of the time series, and not from any physical mechanism.

The characteristics of these spectra, the elevated spectral activity extending from about 0.2 up to 1 with an abrupt drop above, are also common features of frequency spectra obtained from oceanographic data (e.g. Voorhis 1968; Gould 1971 for instance).

The subharmonic excitations seen here are probably attributable to nonlinear interactions combined with the phase-locking tendency of dissipation. However all that we may establish with certainty is that the linear terms in the equations of motion, integrated from random initial conditions, would have power spectra much richer (i.e. many more discrete frequencies) that those of figure 21. To see this, we consider (1)–(3) utilizing the representation (5), with nonlinear terms discarded. The resulting initial-value problem has wave solutions whose frequency density exceeds that shown in figure 21 (a–c) by a factor of at least 10. (The frequency density is just the resonance frequencies of a cavity for gravity waves, whose density of states

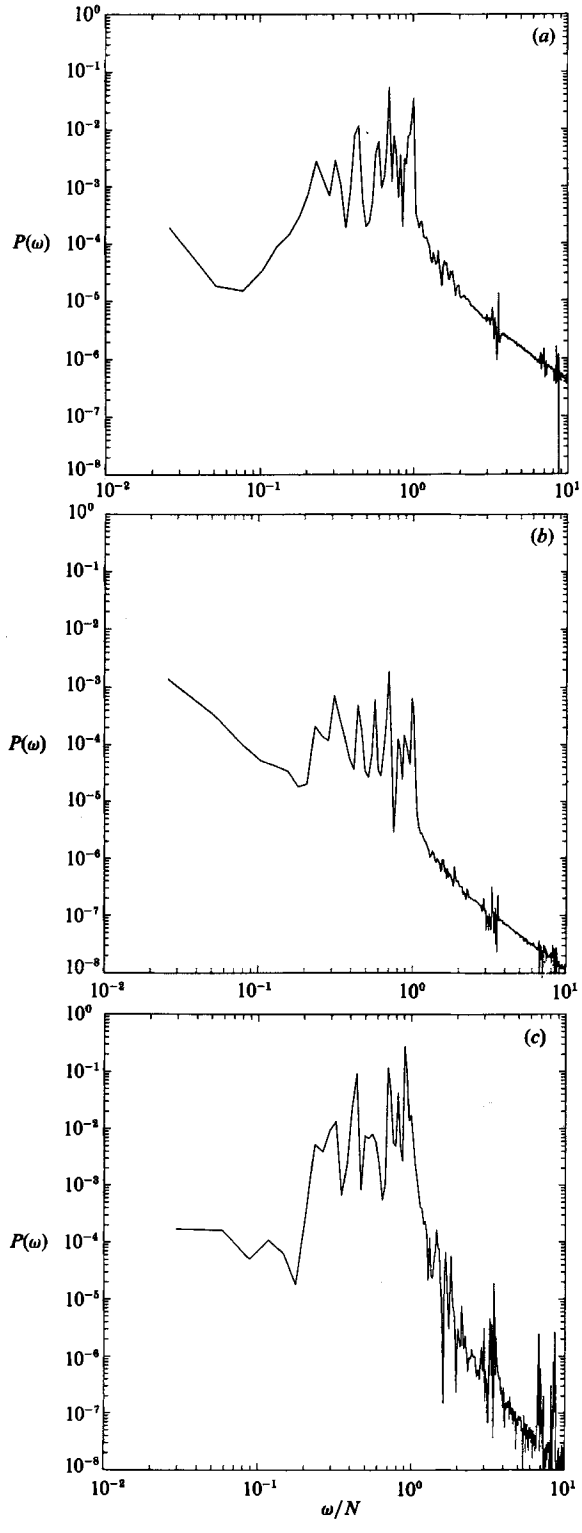

FIGURE 21. Frequency spectra of the potential energy $P(\omega)$ for: (*a*) run 2A, (*b*) 2B and (*c*) 2C. The frequency ω is normalized by N ($N = 2\pi$).

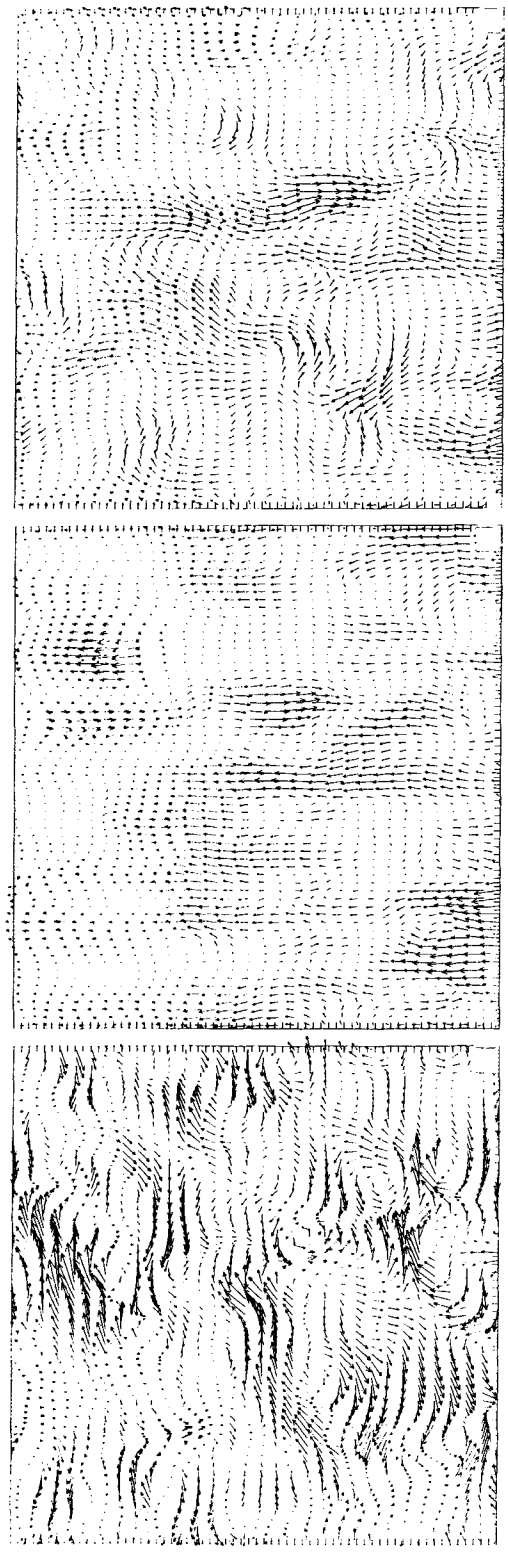

FIGURE 22. Vector plots of $\boldsymbol{u}(x, y, z)$ for (x, z)-slice at the mid planes of the flow, $t = 3.88$. (*a*) run 2A; (*b*) 2B; (*c*) 2C.

corresponds to a 64^3 cubical box.) Moreover, power spectra for runs (3A, 3B) and (4A, 4B), with $N = 4\pi, 20\pi$ do not show an increased density of excitations in the power spectra.

For run 2B (vortical initial conditions), the low-frequency excitation is pronounced, although the time record is too small to compare there results with a possible ω^{-2} slope analytically introduced by Garrett & Munk (1972) and commonly observed in the ocean. (In any case, comparisons with oceanic data are limited because of the absence of rotation in the numerical model.) The lowest frequencies (for case B) seem to be attributable to the Φ_1 turbulence.

It is of interest to note that at small ω and for vortex initial conditions, $P(\omega)$ exceeds the vertical kinetic-energy power spectrum by about an order of magnitude, at least for the vortical initial condition. (For brevity, we do not show the latter spectra.) This result survives high-pass filtering and is qualitatively similar to the oceanographic results (Gould 1971), although we stress again that the present results are for non-rotating flows.

3.3.2. *Spatial structure of the flow*

Figure 22(*a–c*) shows vector plots of $\boldsymbol{u}$ for a vertical slice of the flow, and for runs 2A, 2B, and 2C ($N = 2\pi, t = 3.88$). Figures 22(*a*) and 22(*b*) look similar, except for some vertical eddies due to the higher proportion of Φ_2 energy in the first case. When the initial field is constituted only from vortex motion (run 2B), the horizontal motion clearly dominates, and some definite patches are visible. When the flow is dominated by the waves, the vertical motion is much more pronounced.

3.3.3. *Distribution function for shear*

Since the stability of the flow against vertical overturning is set by some measure of vertical shear, it is of interest to compare the distribution function $\mathscr{P}(x), x = \partial u/\partial z$ for stably stratified flow and isotropic turbulence. Figure 23 compares the $\mathscr{P}(\partial u/\partial z)$ for cases 0B and 4B; i.e. $N = (0, 20\pi)$, vortex initial conditions. The unstratified case has, at the time shown ($t = 3.88$), become essentially isotropic at all wavenumbers. For these curves, $\langle(\partial u/\partial z)^2\rangle^{\frac{1}{2}} = (1.00, 3.00)$ for cases (0B, 4B), respectively. Thus for case 4B, $Ri \sim 400$ (as computed by (21)) is extremely large, indicating strong stability. A striking feature of the isotropic turbulence $\mathscr{P}$ is the near-exponential range extending from $\partial u/\partial z \sim 1.0$ to values such that no resolution remains. We have remarked earlier (Herring & Métais 1989) on the apparent ubiquity of such distributions, but the context of our findings there was a special two-dimensionally forced problem, and the present case of decaying turbulence seems cleaner. But in the more general context, we should note that the exponential distribution occurs for convection (Castaing *et al.* 1989), quasi-geostrophic turbulence (McWilliams 1989), and has been observed for structure functions and vorticity in isotropic turbulence (Anselmet *et al.* 1984; Yamamoto & Hosokawa 1988).

With regard to the *approximate* exponential distribution, we should note that the qualitative differences of these curves from Gaussian (with the same variance) is consistent with the tendency of flows to develop strong gradients in small spatial regions, with quiescent regions (small gradients) becoming the more likely result of a random sampling. This indicates an intermittency, but we do not see here strong evidence of coherent structures, such as values of kurtosis (for vorticity, or temperature) significantly larger than their Gaussian value (3.0). Castaing (1989) has recently suggested that the almost exponential shape is derivable from a log–normal distribution of the dissipation of turbulent patches, with the distribution of the

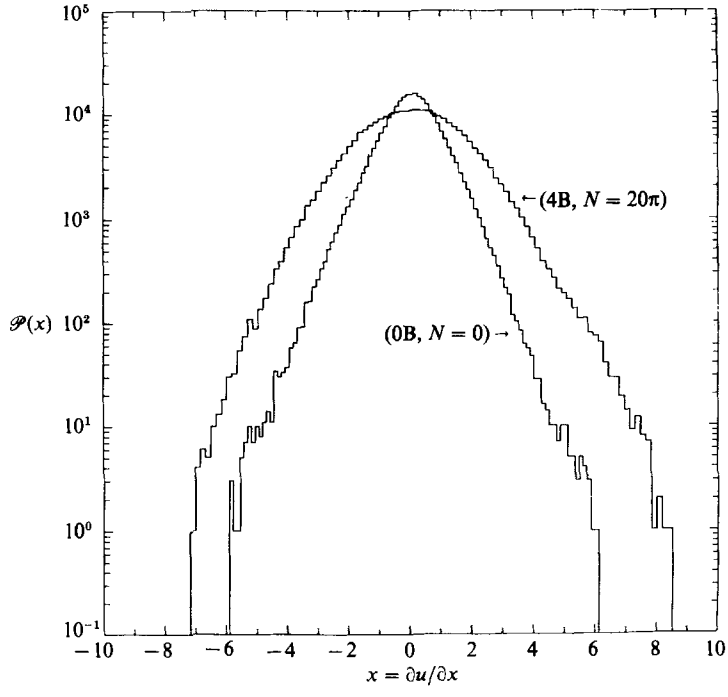

FIGURE 23. Probability distribution density $\mathscr{P}(x), x = \partial u/\partial z$, for cases 0B and 4B. For these, $\langle(\partial u/\partial z)^2\rangle)^{\frac{1}{2}}$ is 1.0 and 3.0 for 0B and 4B respectively. Note that using (21) for $Ri, Ri \sim 400$ for case 4B: overturning instability occurs nowhere, if (21) is a valid criterion for its detection.

intensity of each patch Gaussian. We note that the distribution need not to be so exotic as log–normal: in fact an exponential distribution of variance squared would result in a strict exponential.

4. Conclusion

Summarizing the results for 'weakly stratified' flows, which are here compared to laboratory experiments, we see overall, for statistical parameter such as lengthscales and gross energetics, qualitative agreement between the direct numerical simulation and the laboratory experiments. This suggests that the direct numerical simulations have a satisfactory degree of realism, for most quantities examined. The exception is the heat flux, shown in figure 3. We observe in the direct numerical simulation the familiar damped oscillations about zero, qualitatively the same as in the laboratory experiments. However, in the numerical simulation the earliest excursion of $\langle w\Theta\rangle$ exceeds the laboratory measurements by about a factor of 2. This may well be a consequence of the Prandtl-number differences ($\sigma = 1$ for the numerical simulation, and $\sigma \approx 200$ for the laboratory experiment). We have checked that increasing ν by a factor 2 with the same value of κ decreases the transient excursion but, as noted in the introduction, $\sigma = 200$ at $R_\lambda = 40$ is beyond the range of present computations. Furthermore, the heat flux measured recently in the stratified wind-tunnel grid-turbulence experiments for air ($Pr = 0.7$) by Lienhard (1988) is closer to the numerical simulation than that of Itsweire *et al.* (1986). This trend also fits with the observation that increasing σ decreases the transient excursion.

Comparing (for the numerical simulations) stratified flows with 'equivalent'

unstratified flows, perhaps the most striking difference is that the former exhibits a much smaller transfer to small scale than the latter (cf. figure 11*a*, *b*). This reduction in transfer is in the high (horizontal) wavenumber; it is largely a diminution in the contribution of small-scale wave–vortex interaction to the vortex transfer function. (On the other hand, the vertical transfers (k_z) due to vortex–vortex interaction actually increase somewhat with N, see figure 10*a*, *b*.) This reduced small-scale transfer is responsible for the fact that as N increases, the vortex energy at small scales decreases (see figure 8).

For $N \neq 0$ the horizontal integral scale L_h increases with time much faster than the vertical integral scale L_v (see figure 6*a* and (12) and (13)). For unstratified flows, both lengthscales increase at a rate intermediate between L_v and L_h for the stratified case. The behaviour of L_h would seem to correspond to the energy transfer of vortex energy into the large scales.

The nature of the collapse phase of the turbulence is perhaps best illustrated in terms of the behaviour of the Thorpe scale (see (19) for a definition), which, according to figure 6(*a*) shows a precipitous drop at $Nt \approx 6$. We note from figure 12(*a–f*) that at this time, convolutions in the isothermal surfaces also disappear. This is the same time at which the Ozmidov, Kolmogorov, and Thorpe scales become equal (also shown in figure 6*a*). Finally, at this time, $\Phi_1(t)$ for $N = 0.98$ breaks away from the unstratified Φ_1 curve (see figure 5). The collapse time ($Nt_c \approx 6$) and the corresponding Froude number ($Fr \approx 0.25$) seem to be in accord with the experiments (cf. Hopfinger 1987). The structures that developed after the collapse are not 'coherent' structures in the sense, that, for the latter, the kurtosis of temperature or vorticity is much larger than the Gaussian value of 3. In any case, much higher resolutions may be required for such structure to develop (McWilliams 1984).

The calculations of §3.3 indicate a lack of universality for strongly stratified, dissipative turbulence. Although we note that initial data containing only horizontal motions (case B) do tend to be dominant at strong stratification, the frictional effect associated with vertical variability causes the net energy transfer to be three-dimensional. Hence, the flow has a strong dissipation, atypical of two-dimensional turbulence. Other initial conditions, either wave (case C) or equipartition (case A), survive even in strong stratification and for a long time. This indicates initial-value dependence which seems beyond the scope of simple inviscid equipartitioning ideas. These results are similar to those found in shallow-water equations by Farge & Sadourny (1989). Perhaps these results should not be surprising, in view of the multiple equilibria frequently noted in dynamical systems.

In our discussions of waves and turbulence, we designated ϕ_1 'stratified turbulence' and ϕ_2 'waves'. Such a description is clearly inadequate; it not only leaves out Θ (and its possible wave-like phase relationship to ϕ_2), but also any mention of wave-like oscillations of the (ϕ_2, Θ) degrees of freedom. Despite this over simplification, we note that in practice the vertical vorticity ($\approx \phi_1$) shows little of the ($\omega \approx N$) oscillations characteristic of (ϕ_2, Θ). This suggests not only that the flow quickly reaches a state in which (ϕ_1, ϕ_2) are good first-order discriminators between waves and turbulence, but also that there is, at small Fr, little effective interaction between waves and turbulence. This fact is made more dramatic if we recall that for unstratified turbulence (ϕ_1, ϕ_2) are equipartitioned in about one-eddy circulation time.

Our results here for strongly stratified flows, and for those runs for which the vortical component dominates, may be usefully discussed in the light of Lilly (1983). We recall that Lilly's proposals consisted of two essential ideas. The first is that small-

Fr flows, and their observed strong two-dimensionality, may be understood in terms of a $Fr \to 0$ scaling analysis of the equations of motion similar to that introduced by RMW. Such an analysis yields (in addition to buoyancy waves) two-dimensional turbulence in vertically decoupled layers. The second idea is that as time proceeds, these layers lose their initial coherence, much as strictly two-dimensional turbulence loses predictability. As in the predictability problem, the smallest vertical scales of an initially vertically coherent flow will decorrelate first and the decorrelation then spreads to larger scales. (The r.m.s.) vertical variability increases until limited by the outbreak of three-dimensional dynamical mixing. The latter effects are beyond the low-Fr scaling analysis, at least to the order examined in detail by RMW or Lilly (1983). It may be that the higher-order 'balanced' analysis of McWilliams (1985) is able to give a suitable coupling of the gravity component to the two-dimensional turbulence equations.

Given the general validity of Lilly's picture for the near two-dimensional, $Fr \to 0$ limit, there remains the question: do the present results display the degree of vertical overturning needed to 'glue' the two-dimensional layers together? Clearly, for the strongest stratifications investigated (cases 4A and 4B), we see little evidence of overturning. On the other hand, if the results of figure 23 indicate the (extremely strong) stability of this flow, then, for this case, Lilly's picture is plausible with viscous dissipation (by vertical shear), instead of vertical overturning, removing the energy of the two-dimensional flow. This would explain the impression that the flow is strongly dissipative, despite the fact that it is strongly two-dimensional. We recall in this connection that our $\Phi_1(k_z)$-spectrum shows no trace of a power law, as would be expected if some form of nonlinear effects were determining its shape at low k_z. Moreover, our previous results for forced stratified turbulence (Herring & Métais 1989) did show a k_z^{-3} spectrum for scales below the forcing wavenumber. This would imply that much larger R_λ must be simulated before the atmospheric conditions envisioned by Lilly are reached.

We are grateful to M. Lesieur, J. C. McWilliams and J. J. Riley for many enlightening discussions. These computations were carried out at the Pittsburgh Supercomputer Center. Computing resources were supplied by a grant from the OASC of the National Science Foundation. Part of this work was done when O. Métais was an ASP postdoctoral fellow at NCAR. NCAR is sponsored by the National Science Foundation.

REFERENCES

Anselmet, F., Gagne, Y., Hopfinger, E. J. & Antonia, R. A. 1984 High-order velocity structure functions in turbulent shear flows. *J. Fluid Mech.* **140**, 63–89.

Castaing, B. 1989 Sur la formation des histogrammes en turbulence. *C.R. Acad. Sci. Paris* (submitted).

Castaing, B., Gunaratne, G., Heslot, F., Kadanoff, L., Libchaber, A., Thomae, S., Wu, X.-Z., Zaleski, S. & Zanetti, G. 1989 Scaling of hard thermal turbulence in Rayleigh–Bérnard convection. *J. Fluid Mech.* (in press).

Craya, A. 1958 *Contribution à l'Analyse de la Turbulence Associée à des Vitesse Moyennes.* P. S. T. Ministère de l'Air (Fr), 345 pp.

Dickey, T. D. & Mellor, G. L. 1980 Decaying turbulence in neutral and stratified fluids. *J. Fluid Mech.* **99**, 13–31.

Dillon, T. M. 1982 Vertical overturns: a comparison of Thorpe and Ozmidov length scales. *J. Geophys. Res.* **121**, 27–42.

DOUGHERTY, J. P. 1961 The anisotropy of turbulence at the meteor level. *J. Atmos. Terr. Phys.* **21**, 210–213.

FARGE, M. & SADOURNY, R. 1989 Inertial-gravity wave effects on a decaying two-dimensional turbulence in rotation. *J. Fluid Mech.* (submitted).

GARRETT, C. & MUNK, W. 1972 Space–time scales of internal waves. *Geophys. Fluid Dyn* **2**, 225–264.

GIBSON, C. H. 1980 Fossil temperature, salinity and vorticity turbulence in the ocean. In *Marine Turbulence* (ed. J. C. J. Nihoul), pp. 221–257. Elsevier.

GILL, A. E. 1982 *Atmosphere–Ocean Dynamics.* Academic, 662 pp.

GOULD, W. S. 1971 Spectral characteristics of some deep current records from the eastern North Atlantic. *Phil. Trans. R. Soc. Lond.* A **270**, 437–450.

HERRING, J. R. 1974 Approach of axisymmetric turbulence to isotropy. *Phys. Fluids* **17**, 859–872.

HERRING, J. R. & MÉTAIS, O. 1989 Numerical experiments in forced stably stratified turbulence. *J. Fluid Mech.* **202**, 97–115.

HERRING, J. R., ORSZAG, S. A., KRAICHNAN, R. H. & FOX, D. G. 1974 Decay of two-dimensional homogeneous turbulence. *J. Fluid Mech.* **66**, 417–444.

HERRING, J. R., SCHERTZER, D., LESIEUR, M., NEWMAN, G. R., CHOLLETT, J.-P. & LARCHEVEQUE, M. 1982 A comparative assessment of spectral closures as applied to passive scalar diffusion. *J. Fluid Mech.* **124**, 411–437.

HOPFINGER, E. J. 1987 Turbulence in stratified fluids: a review. *J. Geophys. Res.* **92** (C5), 5287–5303.

HUNT, J. C. R., STRETCH, D. D. & BRITTER, R. E. 1988 Length scales in stably stratified turbulent flows and their use in turbulence models. In *Stably Stratified Flow and Dense Gas Dispersion* (ed. J. S. Puttock), pp. 285–321. Clarendon.

ITSWEIRE, E. C. 1984 Measurements of vertical overturns in a stably stratified turbulent flow. *Phys. Fluids* **27**, 764–766.

ITSWEIRE, E. C., HELLAND, K. N. & VAN ATTA, C. W. 1986 The evolution of grid-generated turbulence in a stably stratified fluid. *J. Fluid Mech.* **162**, 299–338.

LESIEUR, M. 1987 *Turbulence in Fluids.* Nijhoff, 286 pp.

LIENHARD, J. H. V. 1988 The decay of turbulence in thermally stratified flow. Ph.D. Dissertation, University of California at San Diego.

LILLY, D. K. 1983 Stratified turbulence and the mesoscale variability of the atmosphere. *J. Atmos Sci.* **40**, 749–761.

MCWILLIAMS, J. C. 1984 The emergence of isolated vortices in turbulent flows. *J. Fluid Mech.* **146**, 21–43.

MCWILLIAMS, J. C. 1985 A uniformly valid model spanning the regimes of geostrophic and isotropic, stratified turbulence: balanced turbulence. *J. Atmos. Sci.* **42**, 1773–1774.

MCWILLIAMS, J. C. 1989 Statistical properties of decaying geostrophic turbulence. *J. Fluid Mech.* **198**, 199–230.

MÉTAIS, O. J., HERRING, J. R., LESIEUR, M. & CHOLLET, J.-P. 1987 Turbulence in stably stratified fluids: statistical theory and direct numerical simulations. In *Stratified Flows* (ed. E. J. List & G. H. Jirka). Reidel.

ORSZAG, S. A. & PATTERSON, G. S. 1972 Numerical simulation of turbulence. In *Statistical Models and Turbulence* (ed. M. Rosenblatt and C. Van Atta). Lecture Notes in Physics, Vol. 12, pp. 127–147. Springer.

OZMIDOV, R. V. 1965 On the turbulent exchange in a stably stratified ocean. *Izv. Acad. Sci. USSR Atmos. Oceanic Phys.* **1**, 493–497.

PATTERSON, G. S. & ORSZAG, S. A. 1971 Spectral calculations of isotropic turbulence: efficient removal of aliasing interactions. *Phys. Fluids* **14**, 2538–2541.

RILEY, J. J. 1985 A review of turbulence in stably stratified fluids. In *Seventh Symp. on Turbulence and Diffusion, Boulder, Colorado, USA.* Amer. Meteorol. Soc., 377 pp.

RILEY, J. J., METCALFE, R. W. & WEISSMAN, M. A. 1981 Direct numerical simulations of homogeneous turbulence in density stratified fluids. *Proc. AIP Conf. on Nonlinear Properties of Internal Waves* (ed. Bruce J. West), pp. 79–112.

SCHUMANN, U. & HERRING, J. R. 1976 Axisymmetric homogeneous turbulence: a comparison of direct spectral simulations with the direct interaction approximation. *J. Fluid Mech.* **76**, 755–782.

STAQUET, C. & RILEY, J. J. 1989 On the velocity field associated with potential vorticity. *Dyn. Atmos. Oceans* (submitted).

STILLINGER, D. C., HELLAND, K. N. & VAN ATTA, C. W. 1983 Experiments on the transition of homogeneous turbulence to internal waves in a stratified fluid. *J. Fluid Mech.* **131**, 91–122.

THORPE, S. A. 1977 Turbulence and mixing in a Scottish loch. *Phil. Trans. R. Soc. Lond.* A **286**, 125–181.

VOORHIS, A. D. 1968 Measurements of vertical motion and the partition of energy in the New England slope water. *Deep-Sea Res.* **15**, 599–608.

YAMAMOTO, K. & HOSOKAWA, I. 1988 A decaying isotropic turbulence pursued by the spectral method. *J. Phys. Soc. Japan* **57**, 1532.